A class of positive-preserving, energy stable and high order numerical schemes for the Poission-Nernst-Planck system

Waixiang Cao [*], Yuzhe Qin[†], Minqiang Xu[‡]

Abstract: In this paper, we introduce and analyze a class of numerical schemes that demonstrate remarkable superiority in terms of efficiency, the preservation of positivity, energy stability, and high-order precision to solve the time-dependent Poisson-Nernst-Planck (PNP) system, which is as a highly versatile and sophisticated model and accommodates a plenitude of applications in the emulation of the translocation of charged particles across a multifarious expanse of physical and biological systems. The numerical schemes presented here are based on the energy variational formulation. It allows the PNP system to be reformulated as a non-constant mobility H^{-1} gradient flow, incorporating singular logarithmic energy potentials. To achieve a fully discrete numerical scheme, we employ a combination of first/second-order semi-implicit time discretization methods, coupled with either the k-th order direct discontinuous Galerkin (DDG) method or the finite element (FE) method for spatial discretization. The schemes are verified to possess positivity preservation and energy stability. Optimal error estimates and particular superconvergence results for the fully-discrete numerical solution are established. Numerical experiments are provided to showcase the accuracy, efficiency, and robustness of the proposed schemes.

Keywords: Poission-Nernst-planck (PNP) system, positive-preserving, energy stable, error estimates, superconvergence

AMS subject classifications 65M12, 65M15, 65M70

1 Introduction

In this paper, we propose a class of positive-preserving, energy stable and high order numerical schemes for solving the Poisson-Nernst-Planck (PNP) system:

$$\frac{\partial c_i}{\partial t} = \nabla \cdot \left(D_i \left(\nabla c_i + q_i c_i \nabla \phi \right) \right), \qquad \text{in } \Omega, \tag{1.1a}$$

$$-\epsilon^2 \Delta \phi = \sum_{i=1}^{n} q_i c_i, \qquad \text{in } \Omega, \tag{1.1b}$$

$$c_i(0,x) = c_{i0}(x), \qquad \text{in } \Omega, \tag{1.1c}$$

where $c_i := c_i(x,t)$ is the concentration of ith particle, q_i is the valency of ith particle, n is the number of species, ϕ is the electric potential, D_i is the diffusion coefficient of ith particle and ϵ is the dielectric constant respectively.

The Poisson-Nernst-Planck (PNP) system emerges as one of the most ubiquitously and meticulously scrutinized models within the domain of charged particle translocation across a diverse

[*]School of Mathematical Sciences, Beijing Normal University, Beijing 100875, China (caowx@bnu.edu.cn).

[†]School of Mathematics and Statistics, Shanxi University Taiyuan 030006, China.

[‡]Corresponding Author. School of Mathematical Sciences, Zhejiang University of Technology, Hangzhou, 310023, China(mqxu@zjut.edu.cn).

array of physical and biological manifestations. This incorporates the free electrons within semiconductors, as cited in [1, 2, 3]; fuel cells as expounded in [4, 5]; ionic particles in electrokinetic fluids as explicated in [6, 7, 8]; the phase separation and polarization events affiliated with ionic liquids [12] the ion channels extant in cell membranes [9, 10, 11]. The PNP system, with its nonlinearity and strong coupling, makes efficient simulation both highly interesting and extremely challenging. A major hurdle in developing numerical schemes for the PNP equation is ensuring density/concentration positivity (or non-negativity), as negative ion concentrations would violate physical principles and be physically implausible.

It is generally conceded that the solutions of the PNP system are endowed with the properties of mass conservation, positive concentration or density, and energy dissipation. It is highly advantageous and earnestly desired that the numerical solutions preserve as many of the intrinsic PNP system properties as feasible, including mass conservation, positivity, and energy stability. During the past several decades, substantial research endeavors have been dedicated and employed in the sphere of devising efficient, positivity-preserving, and energy-stable numerical schemes for PNP equations. One can refer to [13, 14, 15, 16, 17, 18, 19, 20, 38] for a positive-preserving analysis, to [22, 23, 24, 25] for a convergence analysis, and to [26, 28, 27, 37] for an energy stability analysis. Additionally, [29, 30, 31, 32, 33, 34] can be referred to for other numerical schemes. Nevertheless, none of these works have managed to integrate the properties of mass conservation, positivity, and energy dissipation along with optimal error estimates. Instead, these properties have only been partially fulfilled and addressed thus far. Broadly, it is highly arduous to numerically attain all the features simultaneously. Just recently, Liu et al proposed a finite difference numerical scheme for the PNP equations, which can preserve positivity, uphold energy stability, and guarantee convergence [21]. Within this scheme, all the aforesaid properties are met at the discrete level. However, the temporal precision of this scheme is merely first-order, and the spatial precision is second-order.

The core aim of the current work is to design an effective, positivity-preserving, and energy-stable numerical approach for the PNP system in a broader and more inclusive setting: involving multiple species, achieving high-order accuracy, yielding optimal error estimations, and permitting superconvergence investigations. To achieve this goal, we initially recast the original PNP equation into its equivalent variational form, which guarantees that the discrete solution adheres to the original energy dissipation property. Subsequently, a semi-implicit time discretization is formulated, wherein the mobility function is updated explicitly, while the chemical potential component is handled implicitly. Due to the presence of a singular logarithmic energy potential in the energy variational formulation, the Gauss-Lobatto collocation method is adopted to deal with the logarithmic term during spatial discretization. In regard to the spatial discretization of the elliptic equations, the FEM (for continuous approximation) and the DDG method (for discontinuous approximation) are employed. It has been proved that the fully discrete numerical solution displays positive cell averages and positive values at the collocation points. This positivity characteristic ensures the well-posedness of the numerical scheme. Finally, an optimal rate convergence analysis of the proposed numerical schemes is presented. Through constructing a particular projection of the exact solution, it's proven that the numerical solution has superconvergence towards those projections of the exact solution. Notably, the manifestation of the superconvergence phenomenon for the gradient approximation at Gauss points is being reported for the first time ever.

The principal contribution of the paper lies in that: 1) We show that the fully-discrete solution is positive at Gauss-Lobatto points as well as cell-average. This finding extends the prior positivity analysis in [21, 27] from the cell-average scope to a point-wise level. 2) Unlike the energy stability analysis presented [35, 27], the energy stability discussed in this paper pertains to the original energy functional, rather than a modified or numerically approximated energy. 3) The

schemes simultaneously incorporate the desired properties including mass conservation, positivity, energy stability, optimal error estimates and superconvergence analysis. 4) Some interesting superconvergence results are studied and reported for the PNP equations for the first time. Additionally, it should be noted that the methodology put forward in this paper can also be applied to the multi-dimensional situation.

The remainder of the paper is structured as follows. In Section 2, the fully discrete numerical scheme for the PNP equation (1.1) is presented. In Section 3, the mass conservation and positivity properties of the numerical solution are studied, and it is proven that the discrete solution has positive cell averages and values at Gauss-Lobatto points. In Section 4, the energy stability of our algorithm is proved. Optimal error estimates and some superconvergence results are established in Section 5. Finally, in Section 6, several carefully designed numerical examples are provided to support our theoretical findings.

2 Numerical schemes for the PNP system

Let Ω be a bounded domain in $\mathbb{R}^d$. We first reformulate the PNP system (1.1) into its equivalent form as follow:

$$\frac{\partial c_i}{\partial t} = \nabla \cdot \left(D_i \left(c_i \nabla p_i \right) \right), \qquad x \in \Omega, t > 0, \tag{2.1a}$$

$$p_i = q_i \phi + \log c_i + 1, \qquad x \in \Omega, t > 0, \tag{2.1b}$$

$$-\epsilon^2 \Delta \phi = \sum_{i=1}^{n} q_i c_i, \qquad x \in \Omega, t > 0, \tag{2.1c}$$

$$c_i(0, x) = c_{i0}(x), \qquad x \in \Omega. \tag{2.1d}$$

We consider the periodic boundary condition or the following boundary condition

$$\frac{\partial \phi}{\partial \boldsymbol{n}} = \frac{\partial c_i}{\partial \boldsymbol{n}} = 0, \quad \text{on } \partial\Omega, \tag{2.2}$$

where $\boldsymbol{n}$ represents the unit exterior normal vector on the boundary $\partial\Omega$. To simplify our analysis, we assume $\epsilon = 1, D_i = 1$, and we construct our algorithm based on the periodic boundary condition. Note that this is not essential and our algorithm and analysis can also be extended to the boundary condition (2.2).

2.1 The semi-discrete spatial discretization

Let $\mathcal{T}_h$ be a partition of the polygonal domain Ω, and h denotes the mesh size of all the elements within $\mathcal{T}_h$. Denote by $\mathcal{E}_h$ the edge set of $\mathcal{T}_h$, and let $\mathcal{E}_h^0 \subset \mathcal{E}_h$ be the set of all interior edges. The set of boundary edges is denoted as $\mathcal{E}_h^B$. The diameter of the edge $e \in \mathcal{E}_h$ is denoted as h_e.

For any $e \in \mathcal{E}_h^0$, let K_1 and K_2 be two neighboring elements sharing the common edge e. Denote by $\boldsymbol{n}_e$ the normal vector of e which is assumed to be oriented from K_1 to K_2. For any function w, we denote by $\{w\}$ and $[w]$ the average and the jump of w on e, respectively. That is,

$$\{w\} = \frac{1}{2}(w|_{K_1} + w|_{K_2}), \quad [w] = w|_{K_2} - w|_{K_1}, \text{ on } e \in \partial K_1 \cap \partial K_2.$$

Denote by V_h the discrete finite element space associated with $\mathcal{T}_h$. Here, we consider two classes of semi-discrete spatial discretization for (2.1), namely, the continuous approximation FE method and the discontinuous approximation DDG method.

Denote by L^2_{per} the function space in L^2 space satisfying the periodic boundary condition. Define

$$V_h^d = \{v \in L^2(\Omega) : v|_K \in \mathbb{P}^k \text{or } \mathbb{Q}^k, \forall K \in \mathcal{T}_h\},\ V_h^0 = V_h^d \cap L^2_{per}, \tag{2.3}$$

where $\mathbb{P}^k$ represents the space of polynomial functions of degree at most k, and $\mathbb{Q}^k$ denotes the tensor product polynomial space of degree not more than k for each variable.

Then the DDG method for the PNP system (2.1) is as follows: find $c_{ih}, p_{ih}, \phi_h \in V_h^0$ such that for all $v, w, \theta \in V_h^0$

$$\int_K \partial_t c_{ih} v dx = -\int_K c_{ih} \nabla p_{ih} \nabla v dx + \int_{\partial K} \left(\{c_{ih}\} (\widehat{\partial_n p_{ih}} v + (p_{ih} - \{p_{ih}\}) \partial_n v \right) ds, \tag{2.4}$$

$$\int_K p_{ih} w dx = \int_K \left(q_i \phi_h + \log c_{ih} + 1\right) w dx, \tag{2.5}$$

$$\int_K \nabla \phi_h \nabla \theta dx - \int_{\partial K} \left((\widehat{\partial_n \phi_h} \theta + (\phi_h - \{\phi_h\}) \partial_n \theta \right) ds = \sum_{i=1}^n \int_K q_i c_{ih} \theta dx, \tag{2.6}$$

where $\widehat{\partial_n w}$ denotes the numerical fluxes, which is defined on the interface e by

$$\widehat{\partial_n w} = \beta_0 \frac{[w]}{h_e} + \{\partial_n w\} + \beta_1 h_e [\partial_n^2 w].$$

Here (β_0, β_1) are the coefficients of the penalty (defined later), which should be carefully chosen to ensure the stability or satisfy certain positivity-principle property of the DDG method (see e.g.,[39]).

As for the continuous approximation, we define its associated finite element space as follows:

$$V_h^c = \{v \in C^0(\Omega) : v|_K \in \mathbb{P}^k \text{or } \mathbb{Q}^k, \frac{1}{|\Omega|} \int_\Omega v = const,\ \forall K \in \mathcal{T}_h\},\ \ V_h^1 = V_h^c \cap L^2_{per}. \tag{2.7}$$

Then the semi-discrete FE method for the PNP system (2.1) is: find $c_{ih}, p_{ih}, \phi_h \in V_h^1$ such that for all $v, w, \theta \in V_h^1$

$$\int_\Omega \partial_t c_{ih} v dx = -\int_\Omega c_{ih} \nabla p_{ih} \nabla v dx, \tag{2.8}$$

$$\int_\Omega p_{ih} w dx = \int_\Omega \left(q_i \phi_h + \log c_{ih} + 1\right) w dx, \tag{2.9}$$

$$\int_\Omega \nabla \phi_h \nabla \theta dx = \sum_{i=1}^n \int_\Omega q_i c_{ih} \theta dx. \tag{2.10}$$

2.2 The modified semi-discrete spatial discretization

Due to the logarithmic factor $\log c_{ih}$ appears in (2.5) and (2.9), numerical quadrature is usually required to compute the exact integral $\int_K \log c_{ih} w dx$ in practical calculation. A similar situation applies to (2.4) and (2.8). To avoid this numerical quadrature error, we make slight modifications to our numerical schemes. Specifically, the equations (2.5) and (2.9) are replaced by some collocation conditions, while (2.5) and (2.9) are substituted by the numerical quadrature formulation. To be more precise, we denote by $g_{K,j}, 1 \le j \le n_k$ the collocation points in each $K \in \mathcal{T}_h$ and $\omega_{K,j}$ the corresponding quadrature weights associated with $g_{K,j}$, with n_k being the number of collocation points. Let

$$S_K = \{g_{K,j} : 1 \le j \le n_k\},\ \ S = \{S_K : K \in \mathcal{T}_h\},\ \ S_{\partial K} = S_K \cap \partial K.$$

We should note that the cardinality of set S ought to be equal to the degree of freedom of either V_h^0 or V_h^1 to ensure in order to ensure the well-posedness of the numerical scheme.

Define

$$\langle f,v\rangle_K=\sum_{j=1}^{n_k}(fv)(g_{K,j})\omega_{K,j},\ \ \langle f,v\rangle_{\partial K}=\sum_{g_{K,j}\in S_{\partial K}}(fv)(g_{K,j})\omega_{K,j},\ \langle f,v\rangle=\sum_{K\in\mathcal{T}_h}\langle f,v\rangle_K,$$

$$(f,v)_K=\int_K(fv)dx,\ \ (f,v)_{\partial K}=\int_{\partial K}(fv)ds,\ \ (f,v)=\sum_{K\in\mathcal{T}_h}(f,v)_K.$$

Given any positive function $\psi(x)$, let

$$a_\psi(\cdot,\cdot)=\sum_{\tau\in\mathcal{T}_h}a_{\psi,K}(\cdot,\cdot),$$

where for DDG method,

$$a_{\psi,K}(u,v)=\langle\psi\nabla u,\nabla v\rangle_K-\langle\{\psi\},\widehat{\partial_n u}v+(u-\{u\})\partial_n v\rangle_{\partial K}.$$

And for the FE method,

$$a_{\psi,K}(u,v)=\langle\psi\nabla u,\nabla v\rangle_K.$$

We set $a(\cdot,\cdot)=a_\psi(\cdot,\cdot)$ when $\psi=1$. Define V_h as the discrete finite element space associated with DDG method and FE method, that is, $V_h=V_h^0$ for the DDG and $V_h=V_h^1$ for the FEM.

Then both the modified simi-discrete DDG and FE schemes can be rewritten as: find $c_{ih},p_{ih},\phi_h\in V_h$ such that for all $v,w\in V_h,z\in S$,

$$\langle\partial_t c_{ih},v\rangle_K=-a_{c_{ih}}(p_{ih},v),\tag{2.11}$$

$$p_{ih}(z)=(q_i\phi_h+\log c_{ih}+1)(z),\tag{2.12}$$

$$a(\phi_h,w)=\sum_{i=1}^{n}\langle q_i c_{ih},w\rangle_K.\tag{2.13}$$

In the subsequent part of this paper, our algorithm and theoretical analysis are are perpetually predicated on the modified schemes (2.11)-(2.13).

2.3 The fully-discrete numerical scheme

In this subsection, we propose the first-order and second-order semi-implicit schemes with respect to the time discretization.

The first-order semi-implicit scheme is: given $c_{ih}^m,p_{ih}^m,\phi_h^m\in V_h$, find $c_{ih}^{m+1},p_{ih}^{m+1},\phi_h^{m+1}\in V_h$ such that for all $v,w\in V_h$

$$\langle\frac{c_{ih}^{m+1}-c_{ih}^m}{\tau},v\rangle=-a_{c_{ih}^m}(p_{ih}^{m+1},v),\ \ \forall v\in V_h,\tag{2.14}$$

$$p_{ih}^{m+1}(z)=\left(q_i\phi_h^{m+1}+\log c_{ih}^{m+1}+1\right)(z),\ \ \forall z\in S,\tag{2.15}$$

$$a(\phi_h^{m+1},w)=\langle q_i c_{ih}^{m+1},w\rangle,\ \forall w\in V_h.\tag{2.16}$$

Here $\tau=t_{m+1}-t_m$ denotes the time step size. To obtain the second-order semi-implicit scheme, we make a slight modification to (2.14) as follows:

$$\langle\frac{\frac{3}{2}c_{ih}^{m+1}-2c_{ih}^m+\frac{1}{2}c_{ih}^{m-1}}{\tau},v\rangle=-a_{(2c_{ih}^m-c_{ih}^{m-1})}(p_{ih}^{m+1},v),\ \ \forall v\in V_h.\tag{2.17}$$

Then the second-order semi-implicit numerical scheme is: given $c_{ih}^m,p_{ih}^m,\phi_h^m\in V_h$, find $c_{ih}^{m+1},p_{ih}^{m+1},\phi_h^{m+1}\in V_h$ such that equations (2.15)-(2.17) are satisfied.

3 Mass conservation and positive-preserving

In this section, we study the mass conservation and positive-preserving properties of our fully-discrete numerical schemes. To simplify our analysis and make the idea clearer, in the rest of this paper, we focus on the $\mathbb{Q}^k$ case and the first-order semi-implicit scheme within a two dimensional setting. In addition, the collocation points $g_{K,j}$ are taken as the Gauss-Lobatto points in each element K. i.e.,

$$S_K = \{g_{K,l} = (g_i^x, g_j^y) : 1 \le i, j \le k+1, 1 \le l \le n_K = (k+1)^2\},$$

where g_i^x, g_j^y denote the Gauss-Lobatto points along the x and y directions, respectively. Our subsequent analysis will demonstrate that this special choice of collocation points gives rise to an optimal error estimates as well as some superconvergence properties for the numerical solution.

Multiplying both sides of (2.15) by $\omega_{K,j} w(g_{K,j})$ and summing up over all j result in

$$\langle p_{ih}^{m+1}, w\rangle_K = \langle q_i \phi_h^{m+1} + \log c_{ih}^{m+1} + 1, w\rangle_K. \tag{3.1}$$

Similarly, by taking $w \in V_h$ as the Lagrange basis function associated with $g_{K,j}$, we can obtain (2.15). In other words, the two equations (2.15) and (3.1) are equivalent. Note that the the $(k+1)$-point Gauss-Lobatto numerical quadrature is exact for polynomials of degree not exceeding $2k$, which leads to

$$(w, v)_K = \langle w, v\rangle_K, \quad (w, v)_{\partial K} = \langle w, v\rangle_{\partial K}, \quad \forall w, v \in \mathbb{Q}^{2k}(K). \tag{3.2}$$

Then (2.14)-(2.16) can be reformulated as

$$(\frac{c_{ih}^{m+1} - c_{ih}^m}{\tau}, v) = -a_{c_{ih}^m}(p_{ih}^{m+1}, v), \quad \forall v \in V_h \tag{3.3}$$

$$(p_{ih}^{m+1}, \theta) = (q_i \phi_h^{m+1} + 1, \theta) + \langle \log c_{ih}^{m+1}, \theta\rangle, \quad \forall \theta \in V_h, \tag{3.4}$$

$$a(\phi_h^{m+1}, w) = \sum_{i=1}^{n} (q_i c_{ih}^{m+1}, w), \ \forall w \in V_h. \tag{3.5}$$

3.1 Mass conservation

By substituting $v = 1$ into equation (2.14) and making use of the periodic boundary condition, we can effortlessly derive that

$$\int_\Omega c_{ih}^{m+1} dx = \int_\Omega c_{ih}^m dx = \int_\Omega c_{ih}^0 dx.$$

In other words, the fully-discrete numerical scheme (2.14)-(2.16) possesses the property of mass conservation.

3.2 Positivity-preserving

In this subsection, we shall prove that the fully-discrete numerical scheme has positive cell-average. Subsequently, we will utilize these positive cell-averages to design a positive limiter across the whole domain. Throughout this paper, we adopt standard notations for Sobolev spaces For instance, we have $W^{m,p}(D)$ on a sub-domain $D \subset \Omega$, which is equipped with the norm $\|\cdot\|_{m,p,D}$ and the semi-norm $|\cdot|_{m,p,D}$. When $D = \Omega$, we omit the index D. In the case where $p = 2$, we define $W^{m,p}(D) = H^m(D)$, $\|\cdot\|_{m,p,D} = \|\cdot\|_{m,D}$, and $|\cdot|_{m,p,D} = |\cdot|_{m,D}$. The

notation $A \lesssim B$ implies that A can be bounded by B multiplied by a constant that is independent of the mesh size h and the time step size τ.

We start with some preliminary aspects. Firstly, we define a broken space as follows

$$\mathcal{H}_h = \{v \in L^2 : v|_K \in H^1, \forall K \in \mathcal{T}_h\},$$

and for all $v \in \mathcal{H}_h$, we define

$$\|v\|_E = \left(\sum_{K\in\mathcal{T}_h} \int_K |\nabla v|^2 dx + \sum_{e\in\mathcal{E}_h^0} \int_e \frac{1}{h_e}[v]^2 ds \right)^{\frac{1}{2}}.$$

We note that for the FE method, the energy norm is reduced to the standard semi-norm in the H^1 space due to the continuity in the FE space.

Secondly, we discuss the property of the bilinear form $a_\psi(\cdot,\cdot)$ for the semi-discretezation. We assume that

$$0 < \psi_0 \le \psi \le \psi_1.$$

Recalling the definition of $a_\psi(\cdot,\cdot)$, we can readily derive that

$$|a_\psi(u,v)| \le \psi_1 \langle \nabla u, \nabla u\rangle^{\frac{1}{2}} \langle \nabla v, \nabla v\rangle^{\frac{1}{2}}, \;\; a_\psi(v,v) \ge \psi_0 \langle \nabla v, \nabla v\rangle.$$

By making use of (3.2), we obtain that

$$|a_\psi(w,v)| \le \psi_1 \|w\|_E \|v\|_E, \;\; |a_\psi(v,v)| \ge \psi_0 \|v\|_E^2, \;\; \forall w, v \in V_h.$$

In other words, the bilinear form $a_\psi(\cdot,\cdot)$ is continuous and coercive in the space V_h for the FE method. As for the DDG method, by applying (3.2) once again, we then obtain for all $v \in V_h$,

$$\begin{aligned} a_\psi(v,v) &\ge \sum_{K\in\mathcal{T}_h} \left(\psi_0 \langle \nabla v, \nabla v\rangle_K + \frac{\beta_0\psi_0}{h} \langle [v],[v]\rangle_{\partial K} - \psi_1 \big| \langle 2\{\partial_n v\} + \beta_1 h[\partial_n^2 v], [v]\rangle_{\partial K} \big| \right) \\ &= \sum_{K\in\mathcal{T}_h} \left(\psi_0 (\nabla v, \nabla v)_K + \frac{\beta_0\psi_0}{h} ([v],[v])_{\partial K} - \psi_1 \big| (2\{\partial_n v\} + \beta_1 h[\partial_n^2 v], [v])_{\partial K} \big| \right). \end{aligned}$$

Therefore, if (β_0, β_1) satisfy the stability condition (see, e.g., [39]),

$$\psi_0\beta_0 \ge \psi_1 \Gamma(\beta_1), \;\; \text{with} \;\; \Gamma(\beta_1) = \sup_{\substack{v\in\mathbb{P}_{k-1}(\xi) \\ \xi\in[-1,1]}} \frac{2(v(1) - 2\beta_1 \partial_\xi v(1))^2}{\int_{-1}^1 v^2(\xi) \mathrm{d}\xi}, \tag{3.6}$$

then there exists a positive γ_0 (dependent on ψ_0) such that

$$a_\psi(v,v) \ge \gamma_0 \|v\|_E^2, \;\; \forall v \in V_h. \tag{3.7}$$

Unless otherwise specified, we always assume that the coefficients (β_0, β_1) satisfy the condition (3.6). Similarly, through a direct calculation from the Cauchy-Schwarz inequality and the inverse inequality, we can obtain the following continuity result:

$$|a_\psi(w,v)| \le \gamma_1 \|u\|_E \|v\|_E, \;\; \forall w, v \in V_h. \tag{3.8}$$

Here γ_1 is a positive constant that depends on ψ_1.

Thirdly, we define

$$\tilde{V}_h = \{v \in C^m : v|_K \in \mathbb{Q}_k : \int_\Omega v dx = 0\}$$

where $m = -1$ for the DDG method and $m = 0$ for the FE method. Let $\mathcal{L}_\psi : L^2 \to \tilde{V}_h$ be a operator that satisfies

$$a_\psi(\mathcal{L}_\psi(f), v) = (f, v), \quad \forall v \in \tilde{V}_h. \tag{3.9}$$

Note that when $\psi = 1$, we set $\mathcal{L} = \mathcal{L}_\psi$ for the sake of simplicity. Obviously, given any function $f \in L^2$, there exists a unique $u \in \tilde{V}_h$ such that

$$a_\psi(u, v) = (f, v), \quad \forall v \in \tilde{V}_h.$$

In addition, by utilizing the Poincare inequality along with the coercivity and continuity properties of $a_\psi(\cdot, \cdot)$ in (3.7) and (3.8), we obtain

$$\|\mathcal{L}_\psi(f)\|_0^2 \lesssim |\mathcal{L}_\psi(f)|_1^2 \leq \frac{\gamma_1}{\gamma_0}\|f\|_0\|\mathcal{L}_\psi(f)\|_0, \tag{3.10}$$

which, combined with the inverse inequality, leads to

$$\|\mathcal{L}_\psi(f)\|_{0,\infty} \leq Ch^{-1}\|\mathcal{L}_\psi(f)\|_0 \leq \frac{C\gamma_1}{\gamma_0 h}\|f\|_0. \tag{3.11}$$

Furthermore, we define $\|f\|_{\mathcal{L}_\psi}$ as follows:

$$\|f\|_{\mathcal{L}_\psi} = \sqrt{(f, \mathcal{L}_\psi(f))}.$$

Lemma 3.1. *For any functions $f, v \in L^2$, let L_ψ be the operator defined in (3.9). Then for both the FE method and the DDG method with the coefficient $\beta_1 = 0$,*

$$\frac{1}{2}\frac{d}{ds}\|f + sv\|_{\mathcal{L}_\psi}^2 = (\mathcal{L}_\psi(f), v) + s(v, \mathcal{L}_\psi(v)). \tag{3.12}$$

Proof. Recalling the definition of $\mathcal{L}_\psi$, we have, from a direct calculation,

$$\|f + sv\|_{\mathcal{L}_\psi}^2 = (f, \mathcal{L}_\psi(f)) + s(f, \mathcal{L}_\psi(v) + s(\mathcal{L}_\psi(f), v) + s^2(v, \mathcal{L}_\psi(v)),$$

and thus

$$\begin{aligned}\frac{\mathrm{d}}{\mathrm{d}s}\|f + sv\|_{\mathcal{L}_\psi}^2 &= (f, \mathcal{L}_\psi(v)) + (\mathcal{L}_\psi(f), v) + 2s(v, \mathcal{L}_\psi(v)) \\ &= a_\psi(\mathcal{L}_\psi(f), \mathcal{L}_\psi(v)) + (\mathcal{L}_\psi(f), v) + 2s(v, \mathcal{L}_\psi(v)).\end{aligned}$$

When $\beta_1 = 0$, the bilinear form $a_\psi(\cdot, \cdot)$ is symmetrical for both the DDG and the FE method, and thus

$$a_\psi(\mathcal{L}_\psi(f), \mathcal{L}_\psi(v)) = a_\psi(\mathcal{L}_\psi(v), \mathcal{L}_\psi(f)) = (v, \mathcal{L}_\psi(f)).$$

Then the desired result follows from the last two equations. □

For any function $v \in \mathcal{H}_h$, we define the cell average of v in each element K as follows:

$$\bar{v} = \frac{1}{|K|}\int_K v dx. \tag{3.13}$$

Now, we are prepared to present the positivity-preserving property of the numerical scheme (2.14)-(2.16).

Theorem 3.1. *Assume that c_{ih}^{m+1} is the solution of (2.14)-(2.16) with the coefficient $\beta_1 = 0$ for the DDG discretization. Then for both the FE and DDG methods, the numerical scheme (2.14)-(2.16) is positive preserving in the sense that $\bar{c}_{ih}^{m+1} > 0, c_{ih}^{m+1}(g_{K,j}) > 0$ if $\bar{c}_{ih}^{m} > 0$ and $c_{ih}^{m}(g_{K,j}) > 0$ with $1 \le j \le n_k$ for all $K \in \mathcal{T}_h$.*

Proof. First, denote $a_0 = \frac{1}{|\Omega|}\int_\Omega c_{ih}^m dx$, $\mu_i^m = c_{ih}^m - a_0 \in \tilde{V}_h$, and $\mu = (\mu_1, \cdots, \mu_n)$. We consider an energy functional

$$\begin{aligned} J(\mu) &= \sum_{i=1}^{n} \big(\frac{1}{2\tau}(\mu_i - \mu_i^m, \mathcal{L}_{c_{ih}^m}(\mu_i - \mu_i^m)) + \langle(\mu_i + a_0)\log(\mu_i + a_0), 1\rangle\big) \\ &+ \frac{1}{2}(\sum_{i=1}^{n} q_i(\mu_i + a_0), \mathcal{L}(\sum_{i=1}^{n} q_i(\mu_i + a_0))) \end{aligned}$$

over a admissible set

$$A_h = \{(\mu_1, \cdots, \mu_n) : 0 < (\mu_i + a_0)(g_{K,j}) \le M, 1 \le i \le n, K \in \mathcal{T}_h\} \tag{3.14}$$

with $M = \frac{a_0|\Omega|}{h^2}$. Note that $J(\mu)$ is a strictly convex function. Next, we will prove that there exists a minimizer of $J(\mu)$ over the domain A_h. For any $\delta > 0$, we consider

$$A_{h,\delta} = \{(\mu_1, \cdots, \mu_n) : \delta \le (\mu_i + a_0)(g_{K,j}) \le M - \delta, 1 \le i \le n, K \in \mathcal{T}_h\}. \tag{3.15}$$

Since $A_{h,\delta}$ is a compact set in the hyperplane $H = \{(\mu_1, \cdots, \mu_n) : \int_\Omega \mu_i = 0, 1 \le i \le n\}$ and $J(\mu)$ is a strictly convex function, there exists a minimizer of $J(\mu)$ over $A_{h,\delta}$. The key aspect of the positivity analysis is that such a minimizer could not occur at one of the boundary points if δ is sufficiently small.

We denote by μ^* the minimizer of $J(\mu)$ and assume that the minimizer occurs at the boundary of $A_{h,\delta}$. Without loss of generality, we assume $\mu^*(g_{K_0,j_0}) + a_0 = \delta$. Suppose that μ^* attains its maximum value at the point g_{K_1,j_1}. Utilizing the fact that $\int_\Omega \mu^* = 0$ leads to the conclusion that $\mu^*(g_{K_1,j_1}) \ge 0$.

Now we consider the directional derivative: for any $w \in V_h$, we use (3.12) to derive that

$$\begin{aligned} \frac{\mathrm{d}}{\mathrm{d}s} J(\mu_1^*, \mu_2^*, \ldots, \mu_i^* + sw, \ldots, \mu_n^*)|_{s=0} &= \frac{1}{\tau}(\mathcal{L}_{c_{ih}^m}(\mu_i^* - \mu_i^m), w) + \langle \log(\mu_i^* + a_0) + 1, w\rangle \\ &+ (\mathcal{L}(\sum_{i=1}^{n} q_i(\mu_i + a_0)), w). \end{aligned}$$

Let $l_{K,j} \in V_h$ be the Lagrange basis function corresponding to the points $g_{K,j}$, that is, $l_{K,j}(g_{K,i}) = \delta_{i,j}$, where $\delta_{i,j}$ the Kronecker delta function. Now we choose $w = l_{K,j}$ in the last equation and then get

$$\begin{aligned} \frac{\mathrm{d}}{\mathrm{d}s} J(\mu_1^*, \mu_2^*, \ldots, \mu_i^* + sw, \ldots, \mu_n^*)|_{s=0} &= \frac{1}{\tau}\mathcal{L}_{c_{ih}^m}(\mu_i^* - \mu_i^m)(g_{K,j}) + (\log(\mu_i^* + a_0) + 1)(g_{K,j}) \\ &+ \mathcal{L}(\sum_{i=1}^{n} q_i(\mu_i + a_0))(g_{K,j}), \ \ \forall K \in \mathcal{T}_h, j \in \mathbb{Z}_{k+1}. \end{aligned}$$

Especially, we separately substitute $K = K_0, j = j_0$ and $K = K_1, j = j_1$ into the above equation and then get

$$\begin{aligned} \frac{\mathrm{d}}{\mathrm{d}s} J(\mu_1^*, \mu_2^*, \ldots, \mu_i^* + sw, \ldots, \mu_n^*)|_{s=0} &= \frac{\log(\mu_{K_0,j_0}^* + a_0)}{\log(\mu_{K_1,j_1}^* + a_0)} + \frac{1}{\tau}\mathcal{L}_{c_{ih}^m}(\mu_i^* - \mu_i^m)|_{g_{K_1,j_1}}^{g_{K_0,j_0}} \\ &+ \mathcal{L}(\sum_{i=1}^{n} q_i(\mu_i + a_0))|_{g_{K_1,j_1}}^{g_{K_0,j_0}}. \end{aligned}$$

Here the notation $F(x)|_a^b = F(b) - F(a)$. For the first term, we easily obtain that

$$\frac{\log(\mu^*_{K_0,j_0} + a_0)}{\log(\mu^*_{K_1,j_1} + a_0)} \leq \log\frac{\delta}{a_0}.$$

Denote $\alpha_0 = \min\{c_{ih}^m(g_{K,j})\}$, In accordance with (3.11), we obtain

$$\mathcal{L}_{c_{ih}^m}(\mu_i^* - \mu_i^m)|_{g_{\tau_1,j_1}}^{g_{\tau_0,j_0}} \leq 2C_0\alpha_0^{-1}h^{-1}M, \;\; \mathcal{L}(\sum_{i=1}^{n} q_i(\mu_i^* + a_0))|_{g_{\tau_1,j_1}}^{g_{\tau_0,j_0}} \leq 2nC_0h^{-1}M.$$

Here $C_0 = \frac{C\gamma_1}{\gamma_0}$ with C the same as that in (3.11). Define

$$D_0 = 2C_0h^{-1}M(\alpha_0\tau^{-1} + n).$$

Note that D_0 is a constant when h and τ are fixed. For any fixed h and τ, we can choose a particular $\delta > 0$ small enough so that

$$\log\frac{\delta}{a_0} + D_0 < 0,$$

and thus

$$\frac{\mathrm{d}}{\mathrm{d}s}J(\mu_1^*, \mu_2^*, \ldots, \mu_i^* + sw, \ldots, \mu_n^*)|_{s=0} < 0, \;\; 1 \leq i \leq n.$$

This contradicts the assumption that $J(\mu)$ has a minimum at μ^*. Therefore, the global minimum of $J(\mu)$ over $A_{h,\delta}$ could only potentially occur at an interior point, for $\delta > 0$ sufficiently small. Then we can conclude that there exists a solution $\mu \in A_{h,\delta}$ such that

$$\frac{\mathrm{d}}{\mathrm{d}s}J(\mu + sv)|_{s=0} = 0, \;\; \forall v \in V_h,$$

which is equivalent to the numerical schemes (2.14)-(2.16) . Therefore there exists a numerical solution to (2.14)-(2.16) over the compact domain $A_{h,\delta}$ with point-wise positive values at Gauss-Lobatto points $g_{K,i}$. Since

$$\bar{c}_{ih}^{m+1} = \frac{1}{|K|}\sum_{j=1}^{n_k} w_{K,j}c_{ih}(g_{K,j}) > 0.$$

Then the positivity preserving of numerical solution both at the Gauss-Lobatto points and for the cell average is thus established. □

Remark 3.1. *In order to guarantee the positivity of the initial solution at Gauss points, we adopt the following initial discritization:*

$$c_{ih}^0(g_{K,j}) = c_{i0}(g_{K,j}).$$

That is, $c_{ih}^0 \in V_h$ is chosen as the Gauss-Lobatto interpolation of the initial function $c_i^0(x)$.

3.3 limiter

As stated in Theorem 5.1, $c_{ih}|_K \in \mathbb{Q}^k$ is a high order approximation to the smooth function $c_i(x) > 0$, possessing a positive cell average and positive function values at the Gauss-Lobatto points. Utilizing the positive cell average and $c_{ih}(x)$, we are able to design another polynomial $\tilde{c}_{ih}(x)$, which is also a high order approximation to the smooth function $c_i(x) > 0$ and is positive for all $x \in \Omega$. The process for constructing $\tilde{c}_{ih}(x)$ is detailed below.

$$\tilde{c}_{ih}(x)|_K = \bar{c}_{ih} + \theta(c_{ih}(x) - \bar{c}_{ih}), \quad \theta = \min\{1, \frac{\bar{c}_{ih}}{\bar{c}_{ih} - \min_{x\in K} g_h(x)}\}. \tag{3.16}$$

There holds the following property of $\tilde{c}_{ih}(x)$ (see, e.g., [36]):

$$|\tilde{c}_{ih}(x) - c_{ih}(x)| \le C_k \|c_{ih} - c_i\|_\infty, \quad \min_{x\in K} \tilde{c}_{ih}(x) \ge 0, \quad \frac{1}{|K|}\int_\tau \tilde{c}_{ih}(x)dx = \bar{c}_{ih}. \tag{3.17}$$

The above equation indicate that the constructed $\tilde{c}_{ih}$ does not destroy the solution accuracy. Meanwhile, it maintains the same cell averages and is positive at each point within each element.

Remark 3.2. *We have adjusted the energy functional in the following manner:*

$$\begin{aligned} J(\mu) &= \frac{3}{\triangle t}\sum_{i=1}^{n}(\frac{3}{2}\mu_i - 2\mu_i^m - \mu_i^{m-1}, \mathcal{L}_{c_{ih}^m}(\frac{3}{2}\mu_i - 2\mu_i^m + \mu_i^{m-1})) + \langle(\mu_i + a_0)\log(\mu_i + a_0), 1\rangle \\ &+ \frac{1}{2}(q_i(\mu_i + a_0), \mathcal{L}(q_i(\mu_i + a_0)). \end{aligned}$$

By employing the same arguments utilized for the first order schemes, we achieve the acquisition of the positivity property for the second-order schemes.

4 Energy stability

We first define the following energy function:

$$\begin{aligned} E(c) := E(c_1, \ldots, c_n) &= \sum_{i=1}^{n}\int_\Omega \left(c_i\log c_i + \frac{1}{2}q_i c_i\phi\right)dx \\ &= \sum_{i=1}^{n}\int_\Omega \left(c_i\log c_i + \frac{1}{2}|\nabla\phi|^2\right)dx. \end{aligned}$$

Observing that

$$d_t E = -\sum_{i=1}^{n}\int_\Omega c_i|\nabla p_i|^2 dx \le 0,$$

we conclude that the energy is dissipated over time. Subsequently, we will demonstrate that our fully-discrete numerical scheme maintains energy stability.

Theorem 4.1. *The numerical scheme* (2.14)-(2.16) *is energy stable, provided that the mesh size h is sufficiently small. That is, there holds*

$$E(c_h^{m+1}) \le E(c_h^m). \tag{4.1}$$

Proof. First, by choosing $v = p_{ih}^{m+1}$ in (3.3) yields

$$(c_{ih}^{m+1} - c_{ih}^{m}, p_{ih}^{m+1}) = -\tau a_{c_{ih}^m}(p_{ih}^{m+1}, p_{ih}^{m+1}). \tag{4.2}$$

Second, we utilize (3.4) to derive

$$(c_{ih}^{m+1} - c_{ih}^{m}, p_{ih}^{m+1}) = (q_i\phi_h^{m+1}, c_{ih}^{m+1} - c_{ih}^{m}) + \langle \log c_{ih}^{m+1} + 1, c_{ih}^{m+1} - c_{ih}^{m}\rangle.$$

By applying the Taylor expansion, we easily deduce that

$$\langle \log c_{ih}^{m+1}, c_{ih}^{m+1}\rangle - \langle \log c_{ih}^{m}, c_{ih}^{m}\rangle \le \langle \log c_{ih}^{m+1} + 1, c_{ih}^{m+1} - c_{ih}^{m}\rangle.$$

On the other hand, (3.5) indicates that

$$\begin{aligned}\sum_{i=1}^{n}(q_i\phi_h^{m+1}, c_{ih}^{m+1} - c_{ih}^{m}) &= (\phi_h^{m+1}, \mathcal{L}^{-1}(\phi_h^{m+1}) - \mathcal{L}^{-1}(\phi_h^{m})) \\ &\ge \frac{1}{2}(\phi_h^{m+1}, \mathcal{L}^{-1}(\phi_h^{m+1})) - \frac{1}{2}(\phi_h^{m}, \mathcal{L}^{-1}(\phi_h^{m})).\end{aligned}$$

Here in the second step, we have used the convexity of the norm $(v, \mathcal{L}^{-1}v)$ for any function v. Substituting the last three equations into (4.2), we immediately get

$$E(c_h^{m+1}) - E(c_h^{m}) + \tau a_{c_{ih}^m}(p_{ih}^{m+1}, p_{ih}^{m+1}) = 0. \tag{4.3}$$

Then the desired result (4.1) follows due to the positivity $c_{ih}^m(g_{K,j}) > 0$ and the non-negativity of $a_{c_{ih}^m}(v, v)$. □

5 Optimal error estimates and superconvergence analysis

5.1 Preliminaries and error equations

First, we define the Gauss-Lobatto interpolation $I_h : \mathcal{H}_h \to V_h$ which satisfies the condition:

$$I_h v(g_{K,j}) = v(g_{K,j}), \ \ \forall v \in \mathcal{H}_h, 1 \le j \le n_k, \ K \in \mathcal{T}_h.$$

According to [41, 40], the following approximation properties hold:

$$\|v - I_h v\|_{m,p} \lesssim h^{n-m+\frac{2}{p}-\frac{2}{q}}|v|_{n,q}, \ |(\nabla(v - I_h v), \nabla w)_\tau| \lesssim h^{k+1}|v|_{k+2,\tau}\|\nabla w\|_{0,\tau}. \tag{5.1}$$

Second, let us introduce

$$\tilde{a}_\psi(\cdot,\cdot) = \sum_{K\in\mathcal{T}_h}\tilde{a}_{\psi,K}(\cdot,\cdot),$$

where for DDG method,

$$\tilde{a}_{\psi,K}(u, v) = (\psi\nabla u, \nabla v)_K - (\{\psi\}, \widehat{\partial_n u}v + (u - \{u\})\partial_n v)_{\partial K}.$$

and for FE method

$$\tilde{a}_{\psi,K}(u, v) = (\psi\nabla u, \nabla v)_K.$$

In light of the second inequality of (5.1), for the FE method, we have

$$|\tilde{a}_\psi(u - I_h u, v)| = |\tilde{a}_{\psi-\bar{\psi}}(u - I_h u, v) + \tilde{a}_{\bar{\psi}}(u - I_h u, v)| \lesssim h^{k+1}|u|_{k+2}\|\nabla v\|_0.$$

As for DDG method, if $\beta_1 = \frac{1}{2k(k+1)}$, then (see, e.g., [42])

$$|\tilde{a}(u - I_h u, v)| \lesssim h^{k+1}|u|_{k+2}\|v\|_E,$$

and thus

$$|\tilde{a}_\psi(u - I_h u, v)| \lesssim h^{k+1}|u|_{k+2}\|v\|_E. \tag{5.2}$$

In other words, the inequality (5.2) holds true for both the DDG and FE methods.

Third, leveraging the error associated with the Gauss-Lobatto numerical quadrature, we easily derive the following relationships:

$$(f, v)_K - \langle f, v\rangle_K = (f - I_h f, v)_K, \quad (f, v)_{\partial K} - \langle f, v\rangle_{\partial K} = (f - I_h f, v)_{\partial K},$$

which leads to

$$|a_\psi(u, v) - \tilde{a}_\psi(u, v)| \lesssim h^{k+1}|u|_{k+2}\|v\|_E. \tag{5.3}$$

Given (5.2) and (5.3), we conclude that

$$|a_\psi(u - I_h u, v)| \lesssim h^{k+1}|u|_{k+2}\|v\|_E. \tag{5.4}$$

To establish error estimates at time t_{m+1}, we initially assume that the exact solutions c_i, p_i, ϕ are sufficiently smooth. Since c_i is positive and smooth, we suppose there exist $\delta_0, M_0 > 0$ such that

$$\delta_0 \le \|c_i\|_{0,\infty} \le M_0, \quad \|c_i\|_{r,\infty} \le M_0. \tag{5.5}$$

Utilizing the approximation properties of I_h stated in (5.1), for sufficiently small h, we deduce that,

$$\|I_h c_i\|_{0,\infty} \ge \frac{\delta_0}{2}, \quad \|I_h c_i\|_{1,\infty} \le M_0. \tag{5.6}$$

Furthermore, we need a priori assumption at the previous time step t_m, i.e.,

$$\|c_{ih}^m - I_h c_i^m\|_E \lesssim \tau + h^{k+1}. \tag{5.7}$$

The above assumption will be justified later. Due to (5.7), we have the following boundedness for c_{ih}^m in the L^∞ norm.

$$\|c_{ih}^m - I_h c_i^m\|_{1,\infty} \lesssim h^{-1}\|c_{ih}^m - I_h c_i^m\|_E \lesssim h^{-1}(\tau + h^{k+1}).$$

Assuming that $\tau = \mathcal{O}(h)$, then we have

$$\|c_{ih}^m\|_{1,\infty} \lesssim 1. \tag{5.8}$$

Since

$$\|c_{ih}^m - I_h c_i^m\|_{0,\infty} \lesssim |\ln h|^{\frac{1}{2}}\|c_{ih}^m - I_h c_i^m\|_1 \lesssim |\ln h|^{\frac{1}{2}}(\tau + h^{k+1}),$$

then for sufficiently small τ, h,

$$\|c_{ih}^m\|_{0,\infty} \ge \frac{\delta_0}{4}. \tag{5.9}$$

In the rest of this paper, we will adopt the following notation

$$e_v = v - v_h, \quad \eta_v = v - I_h v, \quad \xi_v = I_h v - v_h, \quad v = c_i, p_i, \phi.$$

For all $v, w \in V_h$, note that the exact solutions satisfy

$$
\begin{aligned}
&(\frac{c_i^{m+1}-c_i^m}{\tau}, v) = -\tilde{a}_{c_i^m}(p_i^{m+1}, v) - \tilde{a}_{(c_i^{m+1}-c_i^m)}(p_i^{m+1}, v) + (\frac{c_i^{m+1}-c_i^m}{\tau} - \partial_t c_i^{m+1}, v),\\
&p_i^{m+1}(g_{K,j}) = (q_i\phi_h^{m+1} + \log c_i^{m+1} + 1)(g_{K,j}),\\
&\tilde{a}(\phi^{m+1}, w) = \sum_{i=1}^{n}(q_i c_i^{m+1}, w).
\end{aligned}
$$

Then we derive the following error equations from (2.15), (3.3) and (3.5)

$$
(\frac{\xi_{c_i}^{m+1}-\xi_{c_i}^m}{\tau}, v) = a_{c_{ih}^m}(p_{ih}^{m+1}, v) - a_{c_i^m}(p_i^{m+1}, v) + I(v),\ \forall v \in V_h, \tag{5.10}
$$

$$
e_{p_i}^{m+1}(g_{K,j}) = (q_i e_\phi^{m+1} + \log c_i^{m+1} - \log c_{ih}^{m+1})(g_{K,j}), \tag{5.11}
$$

$$
\tilde{a}(\phi^{m+1}, w) - a(\phi_h^{m+1}, w) = \sum_{i=1}^{n}(q_i e_{c_i}^{m+1}, w),\ \ \forall w \in V_h, \tag{5.12}
$$

where

$$
\begin{aligned}
I(v) = \ & (\frac{c_i^{m+1}-c_i^m}{\tau} - \partial_t c_i^{m+1}, v) - \tilde{a}_{(c_i^{m+1}-c_i^m)}(p_i^{m+1}, v)\\
+ \ & a_{c_i^m}(p_i^{m+1}, v) - \tilde{a}_{c_i^m}(p_i^{m+1}, v) - (\frac{\eta_{c_i}^{m+1}-\eta_{c_i}^m}{\tau}, v).
\end{aligned} \tag{5.13}
$$

Using the Cauchy-Schwarz inequality, we have

$$
\begin{aligned}
&|(\frac{c_i^{m+1}-c_i^m}{\tau} - \partial_t c_i^{m+1}, v) - (\frac{\eta_{c_i}^{m+1}-\eta_{c_i}^m}{\tau}, v)| \lesssim (\tau + h^{k+1})\|v\|_0,\\
&|\tilde{a}_{(c_i^{m+1}-c_i^m)}(p_i^{m+1}, v)| \lesssim \tau\|v\|_E.
\end{aligned}
$$

Combining these inequalities with equation (5.3), we obtain that

$$
|I(v)| \lesssim (\tau + h^{k+1})\|v\|_E,\ \ \forall v \in V_h. \tag{5.14}
$$

5.2 Error estimates

We begin with the estimate of the numerical solution u_h^{m+1}.

Lemma 5.1. *Assume that the condition (5.5) and the a-priori assumption (5.7) are valid. Suppose that the following inequality holds:*

$$
\frac{\tau}{h^2}(\frac{h^{k+1}}{\tau^{\frac{1}{2}}} + \frac{\sum_{i=1}^n \|\xi_{c_i}^m\|_0}{\tau} + \tau) \le \epsilon, \tag{5.15}
$$

where ϵ is a positive constant that is independent of the mesh size h and time step size τ. Then it follows

$$
\frac{\delta_0}{4} \le \|c_{ih}^{m+1}\|_{0,\infty} \le M_0 + \frac{\delta_0}{4}. \tag{5.16}
$$

Proof. First, choosing $v = \xi_{p_i}^{m+1}$ in (5.10) yields

$$(\frac{\xi_{c_i}^{m+1} - \xi_{c_i}^{m}}{\tau}, \xi_{p_i}^{m+1}) = -a_{c_{ih}^m}(e_{p_i}^{m+1}, \xi_{p_i}^{m+1}) - a_{e_{c_i^m}}(p_i^{m+1}, \xi_{p_i}^{m+1}) + I(\xi_{p_i}^{m+1}), \tag{5.17}$$

where $I(v)$ is defined in (5.13). Next, we rearrange terms to get:

$$\begin{aligned} &(\xi_{c_i}^{m+1}, \xi_{p_i}^{m+1}) + \tau a_{c_{ih}^m}(\xi_{p_i}^{m+1}, \xi_{p_i}^{m+1}) \\ &= (\xi_{c_i}^{m}, \xi_{p_i}^{m+1}) - \tau a_{c_{ih}^m}(\eta_{p_i}^{m+1}, \xi_{p_i}^{m+1}) - \tau a_{e_{c_i^m}}(p_i^{m+1}, \xi_{p_i}^{m+1}) + \tau I(\xi_{p_i}^{m+1}). \end{aligned} \tag{5.18}$$

Utilizing equation (5.11) and the fact that $k+1$ Gauss-Lobatto quadrature is exact for polynomials of degree not more than $2k$, we derive

$$\begin{aligned} (\xi_{p_i}^{m+1}, \xi_{c_i}^{m+1}) = \langle \xi_{p_i}^{m+1}, \xi_{c_i}^{m+1} \rangle &= \langle q_i e_\phi^{m+1} + \log c_i^{m+1} - \log c_{ih}^{m+1}, \xi_{c_i}^{m+1} \rangle \\ &= (q_i \xi_\phi^{m+1}, \xi_{c_i}^{m+1}) + \langle \log c_i^{m+1} - \log c_{ih}^{m+1}, e_{c_i}^{m+1} \rangle. \end{aligned}$$

By using (5.12) and the fact that $a(\phi_h^{m+1}, \xi_\phi^{m+1}) = \tilde{a}(\phi_h^{m+1}, \xi_\phi^{m+1})$, we can further deduce:

$$\sum_{i=1}^{n} (q_i \xi_\phi^{m+1}, \xi_{c_i}^{m+1}) = \sum_{i=1}^{n} (q_i \xi_\phi^{m+1}, e_{c_i}^{m+1} - \eta_{c_i}^{m+1}) = \tilde{a}(e_\phi^{m+1}, \xi_\phi^{m+1}) - \sum_{i=1}^{n} (q_i \eta_{c_i}^{m+1}, \xi_\phi^{m+1}).$$

Combining the last two equations and utilizing the inequality

$$\langle \log c_i^{m+1} - \log c_{ih}^{m+1}, e_{c_i}^{m+1} \rangle \geq 0,$$

we can derive that

$$\sum_{i=1}^{n} (\xi_{p_i}^{m+1}, \xi_{c_i}^{m+1}) \geq \tilde{a}(\xi_\phi^{m+1}, \xi_\phi^{m+1}) + \tilde{a}(\eta_\phi^{m+1}, \xi_\phi^{m+1}) - \sum_{i=1}^{n} (q_i \eta_{c_i}^{m+1}, \xi_\phi^{m+1}).$$

Substituting the above equation into (5.18), we obtain that

$$\tilde{a}(\xi_\phi^{m+1}, \xi_\phi^{m+1}) + \tau \sum_{i=1}^{n} a_{c_{ih}^m}(\xi_{p_i}^{m+1}, \xi_{p_i}^{m+1}) \leq \sum_{i=1}^{n} (q_i \eta_{c_i}^{m+1}, \xi_\phi^{m+1}) + \sum_{i=1}^{n} (\xi_{c_i}^{m}, \xi_{p_i}^{m+1}) - \tilde{a}(\eta_\phi^{m+1}, \xi_\phi^{m+1}) + J,$$

where

$$J = \tau \left(\sum_{i=1}^{n} -a_{c_{ih}^m}(\eta_{p_i}^{m+1}, \xi_{p_i}^{m+1}) - a_{e_{c_i^m}}(p_i^{m+1}, \xi_{p_i}^{m+1}) + I(\xi_{p_i}^{m+1}) \right).$$

Using the coercivity property of the bilinear form $a(\cdot, \cdot)$, the uniformly low boundedness of c_{ih}^m, (5.4), and the a-priori assumption (5.7), we can derive that

$$\|\xi_\phi^{m+1}\|_E^2 + \frac{\delta_0}{4} \tau \sum_{i=1}^{n} \|\xi_{p_i}^{m+1}\|_E^2 \lesssim h^{k+1} \|\xi_\phi^{m+1}\|_E + \sum_{i=1}^{n} \|\xi_{c_i}^{m}\|_0 \|\xi_{p_i}^{m+1}\|_0 + |J|.$$

We next proceed to estimate the term J. Using (5.14) and (5.4) once more, we derive that

$$\begin{aligned} |J| &= \tau \left(\sum_{i=1}^{n} -a_{c_{ih}^m}(\eta_{p_i}^{m+1}, \xi_{p_i}^{m+1}) - a_{\xi_{c_i^m}}(p_i^{m+1}, \xi_{p_i}^{m+1}) + I(\xi_{p_i}^{m+1}) \right) \\ &\lesssim \tau \sum_{i=1}^{n} (\tau + h^{k+1} + \|\xi_{c_i}^{m}\|_0) \|\xi_{p_i}^{m+1}\|_E. \end{aligned}$$

By combining the last two inequalities and using the Poincare inequality, we obtain

$$\|\xi_\phi^{m+1}\|_E^2 + \frac{\delta_0}{4}\tau\sum_{i=1}^n \|\xi_{p_i}^{m+1}\|_E^2 \le Ch^{2k+2} + \tau(\tau + h^{k+1})^2 + \tau^{-1}\sum_{i=1}^n \|\xi_{c_i}^m\|_0^2. \tag{5.19}$$

On the other hand, by choosing $v = \xi_{c_i}^{m+1} - \xi_{c_i}^m$ in (5.10) and using (5.14) and (5.4), we have

$$\begin{aligned}
\|\xi_{c_i}^{m+1} - \xi_{c_i}^m\|_0^2 &= \tau\left(a_{c_{ih}^m}(e_{p_i}^{m+1}, \xi_{c_i}^{m+1} - \xi_{c_i}^m) - a_{e_{c_i}^m}(p_i^{m+1}, \xi_{c_i}^{m+1} - \xi_{c_i}^m) + I(\xi_{c_i}^{m+1} - \xi_{c_i}^m)\right) \\
&\lesssim \tau(\|\xi_{p_i}^{m+1}\|_E + \|e_{c_i}^m\|_0 + \tau + h^{k+1})\|\xi_{c_i}^{m+1} - \xi_{c_i}^m\|_E \\
&\lesssim \frac{\tau}{h}(\|\xi_{p_i}^{m+1}\|_E + \|\xi_{c_i}^m\|_0 + \tau + h^{k+1})\|\xi_{c_i}^{m+1} - \xi_{c_i}^m\|_0.
\end{aligned}$$

Here in the last step, we incorporate the inverse inequality. Using the estimate in (5.19) and the a-priori assumption, we derived the following bound:

$$\|\xi_{c_i}^{m+1} - \xi_{c_i}^m\|_0 \le C\frac{\tau}{h}(\tau^{-\frac{1}{2}}h^{k+1} + \tau^{-1}\sum_{i=1}^n \|\xi_{c_i}^m\|_0 + \tau).$$

Consequently,

$$\|\xi_{c_i}^{m+1}\|_0 \le \|\xi_{c_i}^m\|_0 + \|\xi_{c_i}^{m+1} - \xi_{c_i}^m\|_0 \le C\frac{\tau}{h}(\tau^{-\frac{1}{2}}h^{k+1} + \tau^{-1}\sum_{i=1}^n \|\xi_{c_i}^m\|_0 + \tau).$$

Applying the inverse inequality again, along with (5.15) yields

$$\|\xi_{c_i}^{m+1}\|_{0,\infty} \le Ch^{-1}\|\xi_{c_i}^{m+1}\|_0 \le C\frac{\tau}{h^2}(\frac{h^{k+1}}{\tau^{\frac{1}{2}}} + \frac{\sum_{i=1}^n \|\xi_{c_i}^m\|_0}{\tau} + \tau) \le C\epsilon.$$

Therefore, if (5.15) holds with $C\epsilon \le \frac{\delta_0}{4}$, we conclude that

$$\|c_{ih}^{m+1}\|_{0,\infty} \ge \|I_h c_i^{m+1}\|_{0,\infty} - \frac{\delta_0}{4} \ge \frac{\delta_0}{4}.$$

This finishes our proof. □

Remark 5.1. *The inequalities derived from* (5.7) *and* (5.15)*, reveal that, to maintain the positivity of* c_{ih}^{m+1} *in a point-wise manner, the time mesh size* τ *and the space mesh size* h *must adhere to the relationship*

$$\tau \le ch^2,$$

for some positive constant c*. However, when employing high-order time-discretization methods, such as a second-order scheme, the a-priori assumption* (5.7) *undergoes a modification*

$$\|c_{ih}^m - I_h c_i^m\|_E \lesssim \tau^2 + h^{k+1},$$

whereupon analysis of (5.15) *suggests that*

$$\tau \le ch.$$

In other words, to guarantee positivity in a point-wise manner, the constraint imposed on the time step size for lower-order schemes is considerably more stringent compared to that for higher-order time discretization schemes.

Lemma 5.2. *Assume that (5.5) and the a-priori assumption (5.7) are valid. Then, there exist positive constants $a_i, 0 \le i \le 2$ such that*

$$\sum_{i=1}^{n} a_{c_{ih}^m}(e_{p_i}^{m+1}, \xi_{c_i}^{m+1}) \ge \sum_{i=1}^{n} \left(a_0 \|\xi_{c_i}^{m+1}\|_E^2 - a_1 \|\xi_{c_i}^{m+1}\|_0^2\right) - a_2 h^{2k+2}. \tag{5.20}$$

Proof. Considering the equation (5.11), we can write

$$a_{c_{ih}^m}(e_{p_i}^{m+1}, \xi_{c_i}^{m+1}) = a_{c_{ih}^m}(q_i e_\phi^{m+1} + \log c_i^{m+1} - \log c_{ih}^{m+1}, \xi_{c_i}^{m+1}). \tag{5.21}$$

We next estimate the terms on the right-hand side of (5.21). By choosing $w = \xi_\phi$ in (5.12), we derive that

$$\begin{aligned} \|\xi_\phi^{m+1}\|_E^2 &\lesssim \tilde{a}(\xi_\phi^{m+1}, \xi_\phi^{m+1}) = -\tilde{a}(\eta_\phi^{m+1}, \xi_\phi^{m+1}) + \sum_{i=1}^{n} (q_i e_{c_i}^{m+1}, \xi_\phi^{m+1}) \\ &\lesssim h^{k+1} \|\xi_\phi^{m+1}\|_E + \sum_{i=1}^{n} \|\xi_{c_i}^{m+1}\|_0 \|\xi_\phi^{m+1}\|_0, \end{aligned}$$

and thus

$$\|\xi_\phi^{m+1}\|_E \lesssim \sum_{i=1}^{n} \|\xi_{c_i}^{m+1}\|_0 + h^{k+1}. \tag{5.22}$$

Consequently, we estimate the first term as follows:

$$\begin{aligned} \left| \sum_{i=1}^{n} a_{c_{ih}^m}(q_i e_\phi^{m+1}, \xi_{c_i}^{m+1}) \right| = \left| \sum_{i=1}^{n} a_{c_{ih}^m}(q_i \xi_\phi^{m+1}, \xi_{c_i}^{m+1}) \right| &\lesssim \|\xi_\phi^{m+1}\|_E \sum_{i=1}^{n} \|\xi_{c_i}^{m+1}\|_E \\ &\lesssim \sum_{i=1}^{n} (\|\xi_{c_i}^{m+1}\|_0 + h^{k+1}) \|\xi_{c_i}^{m+1}\|_E. \end{aligned} \tag{5.23}$$

On the other hand, by using the Taylor expansion , there exists a u_i between c_i^{m+1} and c_{ih}^{m+1} such that

$$\log c_i^{m+1} - \log c_{ih}^{m+1} = \frac{1}{u_i} e_{c_i}^{m+1} = \frac{1}{u_i}(\xi_{c_i}^{m+1} + \eta_{c_i}^{m+1}).$$

Then

$$a_{c_{ih}^m}(\log c_i^{m+1} - \log c_{ih}^{m+1}, \xi_{c_i}^{m+1}) = a_{c_{ih}^m}(\frac{\xi_{c_i}^{m+1} + \eta_{c_i}^{m+1}}{u_i}, \xi_{c_i}^{m+1}) = a_{c_{ih}^m}(\frac{\xi_{c_i}^{m+1}}{u_i}, \xi_{c_i}^{m+1}).$$

In light of (5.5) and (5.16), we have,

$$\frac{\delta_0}{4} \le u_i \le M + \frac{\delta_0}{4},$$

which yields, together with (5.9) and the coercivity of $a(\cdot,\cdot)$ in (3.7),

$$a_{c_{ih}^m}(\frac{\xi_{c_i}^{m+1}}{u_i}, \xi_{c_i}^{m+1}) \ge \frac{\delta_0 \gamma_0}{2(M + \frac{\delta_0}{2})} \|\xi_{c_i}^{m+1}\|_E^2.$$

Consequently,

$$a_{c_{ih}^m}(I_h(\log c_i^{m+1} - \log c_{ih}^{m+1}), \xi_{c_i}^{m+1}) \ge \frac{\delta_0 \gamma_0}{2(M + \frac{\delta_0}{2})} \|\xi_{c_i}^{m+1}\|_E^2.$$

Substituting the above inequality, and (5.23) into (5.21) and using the Cauchy-Schwarz inequality, we can derive the desired result (5.20). □

Now we are ready to present the error estimates for the fully-discretization numerical solution.

Theorem 5.1. *Let $c_{ih}^{m+1}, p_{ih}^{m+1}, \phi_h^{m+1}$ be the solution of (2.14)-(2.16) with the coefficient $\beta_1 = \frac{1}{2k(k+1)}$ for the DDG discretization. Assume that (5.5) and the a-priori assumption (5.7) hold true. Then*

$$\|c_i^{m+1} - c_{ih}^{m+1}\|_0 + \|I_h c_i^m - c_{ih}^m\|_E \lesssim \tau + h^{k+1}, \tag{5.24}$$

$$\|\phi^{m+1} - \phi_h^{m+1}\|_0 + \|I_h \phi^m - \phi_h^m\|_E \lesssim \tau + h^{k+1}, \tag{5.25}$$

$$\|p_i^{m+1} - p_{ih}^{m+1}\|_0 \lesssim \tau + h^{k+1}. \tag{5.26}$$

Proof. First, we start by choosing $v = \xi_{c_i}^{m+1}$ in (5.10), which yields that

$$\frac{1}{2\tau}(\|\xi_{c_i}^{m+1}\|_0^2 - \|\xi_{c_i}^m\|_0^2 + \|\xi_{c_i}^{m+1} - \xi_{c_i}^m\|_0^2) + a_{c_{ih}^m}(e_{p_i}^{m+1}, \xi_{c_i}^{m+1}) = a_{e_{c_i}^m}(p_i^{m+1}, \xi_{c_i}^{m+1}) + I(\xi_{c_i}^{m+1}).$$

Using the Cauchy-Schwarz inequality and the a-priori assumption (5.7), we can bound the term $a_{e_{c_i}^m}(p_i^{m+1}, \xi_{c_i}^{m+1})$ as follows:

$$|a_{e_{c_i}^m}(p_i^{m+1}, \xi_{c_i}^{m+1})| \lesssim \|p_i^{m+1}\|_{2,\infty}\|e_{c_i}^m\|_0\|\xi_{c_i}^{m+1}\|_E \lesssim (\tau + h^{k+1})\|\xi_{c_i}^{m+1}\|_E. \tag{5.27}$$

Next, combining (5.20), (5.14) and (5.27) together, we have

$$\frac{1}{2\tau}(\|\xi_{c_i}^{m+1}\|_0^2 - \|\xi_{c_i}^m\|_0^2 + \|\xi_{c_i}^{m+1} - \xi_{c_i}^m\|_0^2) + a_0\|\xi_{c_i}^{m+1}\|_E^2 \le C(\tau + h^{k+1})^2 + \frac{a_0}{2}\|\xi_{c_i}^{m+1}\|_E^2 + C\|\xi_{c_i}^{m+1}\|_0^2,$$

and thus

$$\|\xi_{c_i}^{m+1}\|_0^2 - \|\xi_{c_i}^m\|_0^2 + a_0\|\xi_{c_i}^{m+1}\|_E^2 \lesssim \tau(\tau + h^{k+1})^2 + C\tau\|\xi_{c_i}^{m+1}\|_0^2.$$

Here a_0 is a constant the same as that in (5.20). By using the discrete Gronwall inequality, we derive the desired result (5.24) directly. The inequality (5.25) follows from (5.22), (5.24) and the approximation property of I_h. To obtain the error estimates for the variable p_i, we adopt the error equation (5.11) to derive that

$$\|\xi_{p_i}^{m+1}\|_0 \lesssim \|\xi_\phi^{m+1}\|_0 + \|\log c_i^{m+1} - \log c_{ih}^{m+1}\|_0 \lesssim \|\xi_\phi^{m+1}\|_0 + \|\xi_{c_i}^{m+1}\|_0 \lesssim \tau + h^{k+1}.$$

Then (5.26) follows. □

Remark 5.2. *The error estimates in (5.24)-(5.25) reveal a superconvergence phenomenon for the numerical solutions c_{ih}, ϕ_h superconvergent towards the specially constructed projection of the exact solution $I_h c_i, I_h \phi_h$ in the H^1-norm in space, one-order higher than the optimal convergence rate h^k.*

As a direct consequence of the above theorem, we have the following superconvergence results of the derivative approximation at Gauss points for the numerical solutions c_{ih}, ϕ_h.

Corollary 5.1. *Under the assumptions of Theorem 5.1, he following superconvergence result holds for the numerical solutions c_{ih}^m and ϕ_h^m:*

$$\frac{1}{N}\sum_{K\in\mathcal{T}_h}\sum_{z\in\mathcal{G}}\left(\nabla(c_i^m - c_{ih}^m)^2(z) + \nabla(\phi^m - \phi_h^m)^2(z)\right)^{\frac{1}{2}} \lesssim \tau + h^{k+1}. \tag{5.28}$$

Here $\mathcal{G}$ denotes the set of Gauss points of degree k in the whole domain and N represents its cardinality.

Proof. Initially, by using the inverse inequality, we have

$$\begin{aligned}&\left(\frac{1}{N}\sum_{T\in\mathcal{T}_h}\sum_{z\in\mathcal{G}}\nabla(I_hc_i^m-c_{ih}^m)^2(z)\right)^{\frac{1}{2}}+\left(\frac{1}{N}\sum_{T\in\mathcal{T}_h}\sum_{z\in\mathcal{G}}\nabla(I_h\phi^m-\phi_h^m)^2(z)\right)^{\frac{1}{2}}\\ \leq\ & \|I_hc_i^m-c_{ih}^m\|_E+\|I_h\phi^m-\phi_h^m\|_E\lesssim\tau+h^{k+1}.\end{aligned}$$

Furthermore, as demonstrated in reference [40], for any function u and its interpolation I_hu, the following inequality holds:

$$|\nabla(u-I_hu)(z)|\lesssim h^{k+1}|u|_{k+2,\infty}.$$

Then the desired result follows from the last two inequalities and the triangle inequality. □

6 Numerical Results

In this section, we present some numerical experiments to validate our theoretical findings. In our numerical experiment, we will test various various errors which are defined in Theorem 5.1 and Corollary 5.1. For simplicity, we adopt the following notation

$$\mathrm{e}_A^v=\left(\frac{1}{M}\sum_{T\in\mathcal{T}_h}\left(\int_\tau\nabla(v-v_h)\mathrm{d}x\right)^2\right)^{1/2},\mathrm{e}_G^v=\left(\frac{1}{N}\sum_{T\in\mathcal{T}_h}\sum_{z\in\mathcal{G}}\nabla(v-v_h)^2(z)\right)^{\frac{1}{2}}.$$

to test the superconvergence phenomenon for the variable v with $v=u,\phi,c_i$.

Example 6.1.

In this example, we consider a modified PNP system on $\Omega=[0,1]$, accompanied by source terms, such that an exact solution can be obtained. Specifically, the governing equations of the system are as follows:

$$\begin{aligned}\partial_tc_1&=\partial_x(\partial_xc_1+c_1\partial_x\phi)+f_1,\\ \partial_tc_2&=\partial_x(\partial_xc_2-c_2\partial_x\phi)+f_2,\\ -\partial_x^2\phi&=c_1-c_2+f_3,\end{aligned}$$

where the functions $f_i(t,x)$ are determined by the following exact solution:

$$c_1=10^{-3}(\cos(\pi x)+2)e^{-t},c_2=10^{-3}(\cos(2\pi x)+3/2)e^{-t},\phi=10^{-3}(\cos(2\pi x)-1)e^{-t}.$$

The initial conditions are obtained by computing the exact solutions at $t=0$. For c_i, the boundary conditions meet the zero flux boundary conditions. Regarding ϕ the boundary data satisfies:

$$\phi(t,0)=0,\partial_x\phi(t,1)=0.$$

We address the problem by employing the scheme described in (2.14)-(2.16). Here, the value of k ranges from 1 to 3, and the time step is set as $\Delta t=0.01h^3$. In Table 6.1, we display the L^2 norms of the error e_0 at $t=0.1$, alongside their respective convergence orders. Specifically, for the DDG scheme, we adopt $\beta_0=4$. As for β_1, we choose values of $\frac{1}{4}$, $\frac{1}{12}$ and $\frac{1}{24}$ corresponding to $k=1$, 2, and 3, respectively. Notably, both the DDG and FEM schemes demonstrate optimal convergence rates of $k+1$, aligning with our theoretical predictions presented in Theorem 5.1.

Furthermore, Table 6.2 showcases the superconvergence outcomes of our proposed methodology. It reveals that the derivative approximations at Gauss points for the numerical solutions c_h and ϕ_h, obtained using both DDG and FEM, exhibit an order of $O(h^{k+1})$, thereby validating Corollary 5.1. Moreover, the average cell errors of the derivative $\mathrm{e}_A^{c_i}$ and e_A^{ϕ} for both FEM and DDG also exhibit a superconvergence phenomenon with at least an order of $O(h^{k+1})$. Additionally, we observe that the L^2 error stemming from FEM is marginally higher compared to that of the DDG method. Specifically, for the DDG method, the average H^1 error of c_i is at least of the order $O(h^{k+1})$, whereas for FEM, it remains at $\mathcal{O}(h^{k+1})$.

Finally, we solve this problem by employing the scheme outlined in (2.15)-(2.17), with k varying from 1 to 3 and a time step of $\Delta t = 0.01h^2$. The L^2 norms of the error at $t = 0.1$, alongside their respective convergence orders are presented in Table 6.3, similar optimal convergence results have been observed.

TABLE 6.1. Example 6.1 – Numerical results of the (2.14)-(2.16) with $k = 1, 2, 3$

		DDG				FEM			
k	N	$\|e_{c_1}\|_0$	$\|e_{c_2}\|_0$	$\|e_{p_1}\|_0$	$\|e_\phi\|_0$	$\|e_{c_1}\|_0$	$\|e_{c_2}\|_0$	$\|e_{p_1}\|_0$	$\|e_\phi\|_0$
$k=1$	20	8.75E-6	6.68E-6	4.18E-3	6.63E-6	1.18E-5	8.95E-6	5.43E-3	8.91E-6
	40	2.13E-6	1.68E-6	1.06E-3	1.62E-6	2.99E-6	2.24E-6	1.37E-3	2.23E-6
	80	5.56E-7	4.20E-7	2.67E-4	4.00E-7	7.47E-7	5.60E-7	3.43E-4	5.57E-7
	160	1.39E-7	1.05E-7	6.68E-5	9.94E-8	1.87E-7	1.40E-7	8.56E-5	1.39E-7
	R	2.00	2.00	2.00	2.01	2.00	2.00	2.00	2.00
$k=2$	10	1.49E-6	1.03E-6	9.16E-4	1.01E-6	2.03E-6	1.40E-6	1.20E-3	1.42E-6
	20	1.89E-7	1.25E-7	1.12E-4	1.25E-7	2.55E-7	1.75E-7	1.53E-4	1.79E-7
	40	2.36E-8	1.56E-8	1.39E-5	1.56E-8	3.20E-8	2.20E-8	1.91E-5	2.23E-8
	80	2.95E-9	1.95E-9	1.73E-6	1.95E-9	8.03E-9	2.75E-9	2.39E-6	2.79E-9
	160	3.69E-10	2.44E-10	2.18E-7	2.44E-10	1.01E-9	3.43E-10	2.99E-7	3.49E-10
	R	3.00	3.00	3.00	3.00	3.00	3.00	3.00	3.00
$k=3$	10	6.91E-8	4.41E-8	5.28E-5	3.77E-8	7.69E-8	5.83E-8	6.96E-5	5.29E-8
	20	4.36E-9	2.64E-9	3.89E-6	2.34E-9	4.85E-9	3.70E-9	4.41E-6	3.33E-9
	40	2.73E-10	1.64E-10	2.45E-7	1.44E-10	3.04E-10	2.28E-10	2.76E-7	2.09E-10
	80	1.70E-11	1.03E-11	1.53E-8	9.00E-11	1.90E-11	1.41E-11	1.73E-8	1.35E-11
	160	1.07E-12	6.44E-13	9.56E-10	5.63E-12	1.19E-12	8.82E-13	1.08E-9	8.44E-12
	R	4.00	4.00	4.00	4.00	4.00	4.00	4.00	4.00

Example 6.2.

This example is to test the spatial accuracy of our scheme in a 2D setting. Similar to the Numerical Test 5.1 in [2], we consider the PNP problem (2.1) on $\Omega = [0, \pi]^2$ with source terms, i.e.,

$$\begin{aligned}
\partial_t c_1 &= \nabla \cdot (\nabla c_1 + c_1 \nabla \phi) + f_1, \\
\partial_t c_2 &= \nabla \cdot (\nabla c_2 - c_2 \nabla \phi) + f_2, \\
-\Delta \phi &= c_1 - c_2 + f_3,
\end{aligned}$$

where the functions $f_i(t, x, y)$ are determined by the following exact solution

$$\begin{aligned}
c_1(t, x, y) &= 10^{-3}(e^{-10^{-3}t} \cos(x) \cos(y) + 1), \\
c_2(t, x, y) &= 10^{-3}(e^{-10^{-3}t} \cos(x) \cos(y) + 1), \\
\phi(t, x, y) &= 10^{-3} e^{-10^{-3}t} \cos(x) \cos(y).
\end{aligned}$$

TABLE 6.2. Example 6.1 – Superconvergence results of the (2.14)-(2.16) with $k = 1, 2, 3$

		DDG				FEM			
k	N	$\mathrm{e}_A^{c_1}$	$\mathrm{e}_A^{c_2}$	e_A^{ϕ}	$\mathrm{e}_G^{c_1}$	$\mathrm{e}_A^{c_1}$	e_A^{ϕ}	$\mathrm{e}_G^{c_1}$	$\mathrm{e}_{1,G}^{\phi}$
$k=1$	20	1.91E-6	1.53E-6	2.63E-6	4.63E-5	6.17E-7	8.57E-12	1.83E-5	1.81E-5
	40	2.40E-7	1.99E-7	4.37E-7	1.18E-5	1.55E-7	2.15E-12	4.57E-6	4.52E-6
	80	3.00E-8	2.51E-8	7.48E-8	2.96E-6	3.89E-8	5.39E-13	1.14E-6	1.13E-6
	160	3.76E-9	3.14E-9	1.30E-8	7.40E-7	9.73E-9	1.35E-13	2.85E-7	2.84E-7
	Rate	3.00	3.00	2.50	2.00	2.00	2.00	2.00	2.00
$k=2$	10	2.95E-7	2.29E-7	1.94E-7	8.11E-6	2.21E-7	2.17E-11	1.83E-6	1.84E-5
	20	1.32E-8	9.77E-9	8.22E-9	8.19E-7	1.42E-8	1.44E-12	2.31E-7	2.31E-6
	40	4.26E-10	3.25E-10	3.56E-10	9.76E-8	8.93E-10	9.34E-14	2.90E-8	2.90E-7
	80	1.35E-11	1.03E-11	1.56E-11	1.21E-8	5.58E-11	5.84E-15	3.63E-9	3.63E-8
	160	4.22E-13	3.28E-13	6.63E-13	1.51E-9	3.49E-12	3.14E-15	4.54E-10	4.54E-10
	Rate	5.00	5.00	4.55	3.00	4.00	4.00	3.00	3.00
$k=3$	10	1.49E-7	1.05E-7	9.71E-8	4.21E-6	2.57E-8	1.47E-12	1.31E-6	1.32E-6
	20	8.89E-9	6.22E-7	4.15E-9	3.57E-7	1.61E-9	9.19E-14	8.29E-8	8.29E-8
	40	3.61E-10	2.57E-10	1.64E-10	2.41E-8	1.01E-10	5.74E-15	5.18E-9	5.18E-9
	80	1.13E-11	8.08E-12	6.53E-12	1.50E-9	6.31E-12	4.35E-15	3.24E-10	3.24E-10
	Rate	5.00	5.00	4.75	4.00	4.00	4.00	4.00	4.00

TABLE 6.3. Example 6.1 – Numerical results of the (2.15)-(2.17) with $k = 1, 2, 3$

		DDG				FEM			
k	N	$\|e_{c_1}\|_0$	$\|e_{c_2}\|_0$	$\|e_{p_1}\|_0$	$\|e_{\phi}\|_0$	$\|e_{c_1}\|_0$	$\|e_{c_2}\|_0$	$\|e_{p_1}\|_0$	$\|e_{\phi}\|_0$
$k=1$	20	7.29E-7	4.95E-7	2.79E-4	5.10E-7	1.07E-6	6.86E-7	4.02E-4	6.52E-7
	40	1.84E-7	1.24E-7	6.97E-5	1.27E-7	2.68E-7	1.72E-7	1.01E-4	1.67E-7
	80	4.59E-8	3.11E-8	1.74E-5	3.19E-8	6.70E-8	4.29E-8	2.51E-5	4.18E-8
	160	1.15E-8	7.78E-9	4.35E-6	7.96E-9	1.68E-8	1.07E-8	6.28E-6	1.05E-8
	R	2.00	2.00	2.00	2.01	2.00	2.00	2.00	2.00
$k=2$	20	6.27E-8	4.29E-8	2.23E-5	5.65E-8	8.46E-8	6.24E-8	3.02E-5	7.23E-8
	40	7.89E-9	5.24E-9	2.79E-6	7.06E-9	1.06E-8	7.80E-9	3.79E-6	9.06E-9
	80	9.86E-10	6.55E-10	3.49E-7	8.83E-10	1.33E-9	9.75E-10	4.72E-7	1.13E-9
	160	1.23E-10	8.19E-11	4.36E-8	1.10E-10	1.65E-10	1.22E-10	5.90E-8	1.42E-10
	R	3.00	3.00	3.00	3.00	3.00	3.00	3.00	3.00
$k=3$	20	1.35E-9	9.63E-10	9.44E-7	1.16E-9	1.93E-9	1.61E-9	1.04E-6	2.32E-9
	40	8.54E-11	6.02E-11	5.90E-8	4.50E-11	1.21E-10	1.01E-10	6.50E-8	1.45E-10
	80	5.34E-12	3.76E-12	3.68E-9	2.83E-12	7.50E-12	6.31E-12	4.10E-9	9.10E-12
	160	3.37E-13	2.35E-13	2.30E-10	1.77E-13	4.71E-13	3.93E-13	2.54E-10	5.66E-13
	R	4.00	4.00	4.00	4.00	4.00	4.00	4.00	4.00

The initial conditions are obtained by evaluating the exact solution at $t = 0$, and the boundary conditions of c_i and ϕ satisfy the zero flux boundary conditions (2.2).

The L^2-norm errors and their respective orders, with $k = 1$ and 2 at $t = 0.01$, are reported in Table 6.4. Upon these findings, we confirm that both the DDG and FEM exhibit an order of $\mathcal{O}(h^{k+1})$ in space, aligning perfectly with our theoretical expectations outlined in Theorem 5.1. Mirroring the trends observed in 6.1, the L^2 errors errors reported by FEM are marginally higher compared to those attained by the DDG approach. Table 6.5 displays the numerical outcomes related to the derivative approximation at Gauss points and the average cell errors of the derivative. It reveals that these errors, for both the FEM method and the DDG approach, exhibit a superconvergence phenomenon with an order of at least $O(h^{k+1})$, further reinforcing the robustness and

accuracy of our proposed methods.

TABLE 6.4. Example 6.2 – Numerical results of the (2.14)-(2.16) with $k = 1, 2$

		DDG				FEM			
k	N	$\|e_{c_1}\|_0$	$\|e_{c_2}\|_0$	$\|e_{p_1}\|_0$	$\|e_\phi\|_0$	$\|e_{c_1}\|_0$	$\|e_{c_2}\|_0$	$\|e_{p_1}\|_0$	$\|e_\phi\|_0$
$k=1$	5	9.76E-5	9.76E-5	4.18E-3	5.94E-4	1.24E-4	1.24E-4	7.20E-2	1.49E-4
	10	2.51E-5	2.51E-5	1.06E-3	1.51E-5	3.17E-5	3.17E-5	1.85E-2	3.94E-5
	20	6.34E-6	6.34E-6	2.67E-4	5.83E-6	7.96E-6	7.96E-6	4.67E-3	9.99E-6
	40	1.59E-6	1.59E-6	6.68E-5	1.49E-6	1.99E-6	1.99E-6	1.17E-3	2.51E-6
	80	3.98E-7	3.98E-7	1.67E-5	3.73E-7	4.98E-7	4.98E-7	2.93E-4	5.38E-7
	R	2.00	2.00	2.00	2.01	2.00	2.00	2.00	2.00
$k=2$	5	3.17E-6	3.17E-6	1.99E-3	3.13E-6	8.20E-6	8.21E-6	4.98E-3	8.28E-6
	10	1.96E-7	1.96E-7	2.53E-4	3.92E-7	1.06E-6	1.06E-6	6.69E-4	1.07E-6
	20	4.95E-8	4.95E-8	3.19E-5	4.92E-8	1.35E-7	1.35E-7	8.47E-5	1.34E-7
	40	6.19E-9	6.19E-9	3.99E-6	6.15E-9	1.71E-8	1.71E-8	1.06E-5	1.68E-8
	R	3.00	3.00	3.00	3.00	3.00	3.00	3.00	3.00

TABLE 6.5. Example 6.2 – Superconvergence results of the (2.14)-(2.16) with $k = 1, 2$

		DDG				FEM			
k	N	$\mathrm{e}_A^{c_1}$	$\mathrm{e}_A^{c_2}$	e_A^{ϕ}	$\mathrm{e}_G^{c_1}$	$\mathrm{e}_A^{c_1}$	e_A^{ϕ}	$\mathrm{e}_G^{c_1}$	e_G^{ϕ}
$k=1$	5	2.27E-5	2.27E-5	9.96E-5	5.48E-5	2.34E-5	4.63E-5	4.64E-5	6.92E-5
	10	6.70E-6	6.70E-6	8.68E-6	1.51E-5	5.98E-6	1.24E-6	1.18E-5	1.81E-5
	20	1.70E-6	1.70E-6	2.22E-6	3.83E-6	1.50E-6	3.15E-6	2.96E-6	4.56E-6
	40	4.28E-7	4.28E-7	5.62E-7	9.58E-7	3.77E-7	7.92E-7	7.39E-6	1.15E-6
	80	1.07E-7	1.07E-7	1.41E-7	2.39E-7	9.43E-8	1.99E-7	1.85E-7	2.88E-7
	R	2.00	2.00	2.00	2.00	2.00	2.00	2.00	2.00
$k=2$	5	1.00E-7	1.00E-7	7.02E-7	9.49E-8	2.37E-7	5.30E-7	4.72E-7	7.23E-7
	10	1.34E-8	1.34E-8	1.10E-7	4.64E-8	3.03E-8	6.40E-8	6.04E-8	9.16E-8
	20	9.49E-10	9.49E-10	1.39E-8	5.56E-9	3.78E-9	8.05E-9	7.61E-9	1.15E-8
	40	6.01E-11	6.01E-11	1.75E-9	6.95E-10	4.73E-10	1.01E-9	9.51E-10	1.44E-9
	R	4.00	4.00	3.00	3.00	3.00	3.00	3.00	3.00

Example 6.3.

We test our scheme for the 2D PNP system (2.1) with $m = 2$ on the domain $[0, 1]^2$,

$$\begin{aligned}
&\partial_t c_1 = \nabla \cdot (\nabla c_1 + c_1 \nabla \psi),\\
&\partial_t c_2 = \nabla \cdot (\nabla c_2 - c_2 \nabla \psi),\\
&-\partial_x^2 \phi = c_1 - c_2,
\end{aligned}$$

subjects to

$$\begin{aligned}
&c_1(t, x, y) = \frac{1}{20}(\pi \sin(\pi x) + \pi \sin(\pi y)),\\
&c_2(t, x, y) = 3(x^2(1-x)^2 + y^2(1-y)^2),\\
&\frac{\partial c_i}{\partial n} + q_i c_i \frac{\partial \phi}{\partial_n} = 0, (x, y) \in \partial\Omega,\\
&\phi = 0 \text{ on } \Omega_D, \text{ and } \partial_n \phi = 0 \text{ on } \Omega_N,
\end{aligned}$$

where $\partial\Omega_D = \{(x, y) \in \Omega, x = 0, x = 1\}$ and $\partial\Omega_N = \partial\Omega \backslash \partial\Omega_D$.

For $t \in [0, 1]$, Figure 6.1 depicts the minimum cell averages of c_1, c_2, along with the smallest values of c_1 and c_2 at the collocation points, calculated using a 20×20 mesh and various time steps of $\Delta t = 10^{-4}$ and $\Delta t = 10^{-5}$. From Figure 6.1, it is evident that when these values are far apart from $t = 0$, both the smallest cell averages of c_1 and c_2, as well as the minimum values of c_1 and c_2 at the collocation points remain positive, even utilizing a larger time step.

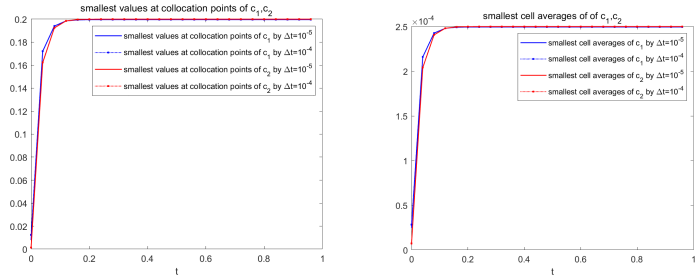

Fig. 6.1. Example 6.3, smallest cell averages and values at collocation points of c_1 and c_2

To gain a deeper insight into the behavior near $t = 0$, we revisited the problem for t within the interval $[0, 10^{-5}]$ utilizing a finer 40×40 mesh and a very small time step of $\Delta t = 10^{-7}$. The smallest cell averages and values at collocation points of c_1 and c_2 are presented in Figure 6.2, which demonstrate that our numerical scheme successfully preserves positivity without the need for a limiter.

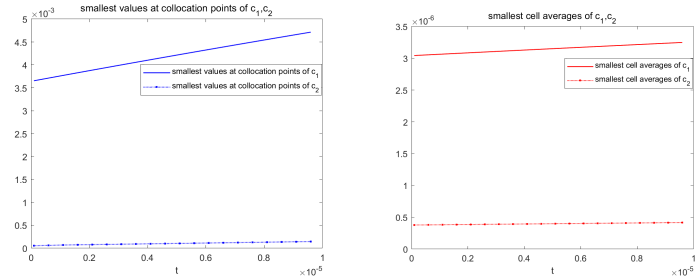

Fig. 6.2. Example 6.3, smallest cell averages and values at collocation points of c_1 and c_2

We meticulously simulate the evolution of c_1, c_2, and ϕ over the time interval $t \in [0, 0.5]$. Figure 6.3 displays the contours of $c_1 - 0.2$ (first column), $c_2 - 0.2$ (second column), and ϕ (right) at $t = 0, 0.01, 0.1$ and 0.5. We discern a remarkable similarity between the contours at $t = 0.1$ and $t = 0.5$, indicating that the system's behavior becomes increasingly uniform as it nears the end of the simulated period. This observation is consistent with the system's apparent progression towards a steady-state configuration, characterized by the values $c_1 = 0.2$, $c_2 = 0.2$ and $\phi = 0$.

Figure 6.4 exhibits the dynamics of both energy decay, evident in the changes recorded on the right vertical axis, and the conservation of mass, as indicated by the left vertical axis. This comprehensive illustration provides clear evidence supporting the fundamental principles of mass conservation and energy dissipation within the system.

7 Concluding remarks

In this work, we systematically introduce and conduct an in-depth analysis of a particular class of numerical schemes that are specifically designed to tackle the time-dependent Poisson-Nernst-

Planck (PNP) system. The fully discrete numerical scheme combines first/second-order semi-implicit time discretization with either the k-th order direct discontinuous Galerkin or finite element method for spatial discretization.

Through rigorous mathematical proofs and derivations, we have demonstrated that the two newly proposed numerical schemes possess essential physical characteristics. Notably, they both ensure the preservation of positivity, which is fundamental to maintaining the physical plausibility of the solutions. Additionally, they exhibit excellent energy stability, guaranteeing the reliability and consistency of the numerical simulations over extended periods. Moreover, we have successfully established the optimal error estimates, which provide a precise quantification of the approximation accuracy of the numerical solutions. Simultaneously, we have uncovered superconvergence results, highlighting the enhanced computational performance of our proposed schemes. A comprehensive series of carefully designed numerical examples have been carried out to validate our theoretical claims.

Ongoing research topics include the construction and analysis of the coupled system of the PNP equations and the Cahn-Hilliard equations.

Acknowledgments

The work is supported by National Natural Science Foundation of China (No. 12271482,12271049, 12326346, 12326347,12201369), and Zhejiang Provincial Natural Science Foundation of China (No. ZCLY24A0101).

References

[1] J.W. Jerome, Analysis of Charge Transport, Mathematical Theory and Approximation of Semi-conductor Models, Springer-Verlag, New York, 1995.

[2] P.A. Markowich, The Stationary Seminconductor Device Equations, Springer-Verlag, Vienna, Austria, 1986.

[3] P.A. Markowich, C.A. Ringhofer, and C. Schmeiser, Seminconductor Equations, Springer Verlag, New York, 1990.

[4] I. Nazarov and K. Promislow, The impact of membrane constraint on PEM fuel cell water management, J. Electrochem. Soc. 154(7): 623-630(2007).

[5] K. Promislow and J.M. Stockie, Adiabatic relaxation of convective-diffusive gas transport in a porous fuel cell electrode, SIAM J. Appl. Math. 62(1): 180–205(2001).

[6] Y. Ben and H.C. Chang, Nonlinear Smoluchowski slip velocity and micro-vortex generation, J. Fluid. Mech. 461: 229-238(2002).

[7] R.J. Hunter, Foundations of Colloid Science, Oxford University Press, Oxford, UK, 2001.

[8] J. Lyklema, Fundamentals of Interface and Colloid Science, Volume II: Solid-liquid Interfaces, Academic Press Limited, San Diego, CA, 1995.

[9] M.Z. Bazant, K. Thornton, and A. Ajdari, Diffffuse-charge dynamics in electrochemical systems, Phys. Rev. E. 70(2): 021506(2004).

[10] B. Eisenberg, Y. Hyon, and C. Liu, Energy variational analysis of ions in water and channels: Field theory for primitive models of complex ionic fluids, J. Chem. Phys. 133(10): 104104(2010).

[11] R.S. Eisenberg, Computing the fifield in proteins and channels, J. Mem. Biol. 150:1-25(1996).

[12] N. Gavish and A. Yochelis, Theory of phase separation and polarization for pure ionic liquids, J. Phys. Chem. Lett. 7:1121-1126(2016).

[13] D. He, K. Pan, and X. Yue, A positivity preserving and free energy dissipative difference scheme for the Poisson-Nernst-Planck system, J. Sci. Comput. 81: 436–458(2019).

[14] Y.Qian, C.Wang, and S.Zhou, A positive and energy stable numerical scheme for the Poisson-Nernst-Planck-Cahn-Hilliard equations with steric interactions, J. Comput. Phys.426: 109908(2021).

[15] J. Shen and J. Xu, Unconditionally positivity preserving and energy dissipative schemes for Poisson-Nernst-Planck equations, Numer. Math.148: 671-697(2021).

[16] F. Huang and J. Shen, Bound/Positivity preserving and energy stable scalar auxiliary variable schemes for dissipative systems: applications to Keller-Segel and Poisson-Nernst-Planck equations, SIAM J. Sci. Comput.43:A1832-A1857(2021).

[17] J. Hu and X. Huang, A fully discrete positivity-preserving and energy-dissipative finite difference scheme for Poisson-Nernst-Planck equations, Numer. Math. 145: 77-115(2020).

[18] J. Ding, Z. Wang, and S. Zhou, Positivity preserving finite difference methods for Poisson Nernst-Planck equations with steric interactions: Application to slit-shaped nanopore conductance, J. Comput. Phys. 397:108864(2019).

[19] J. Ding, Z. Wang, and S. Zhou, Structure-preserving and efficient numerical methods for iontransport, J. Comput. Phys. 418:109597(2020).

[20] F. Siddiqua, Z. Wang, and S. Zhou, A modifified Poisson-Nernst-Planck model with excluded volume effect: Theory and numerical implementation, Commun. Math. Sci.16:251-271(2018).

[21] C. Liu, C. Wang, S. M. Wise, X. Yue, and S. Zhou, A positivity-preserving, energy stable and convergent numerical scheme for the Poisson-Nernst-Planck system, Math. Comput. 90:2071-2106(2021).

[22] J. Ding, C. Wang, and S. Zhou, Optimal rate convergence analysis of a second order numerical scheme for the Poisson-Nernst-Planck system, Numer. Math. Theor. Meth. Appl.12:607-626(2019).

[23] H. Gao and D. He, Linearized conservative finite element methods for the Nernst-Planck-Poisson equations, J. Sci. Comput. 72:1269-1289(2017).

[24] A. Prohl and M. Schmuck, Convergent discretizations for the Nernst-Planck-Poisson system, Numer. Math. 111:591–630(2009).

[25] Y. Sun, P. Sun, B. Zheng, and G. Lin, Error analysis of finite element method for Poisson-Nernst-Planck equations, J. Comput. Appl. Math. 301:28–43(2016).

[26] A. Flavell, J. Kabre, and X. Li, An energy-preserving discretization for the Poisson-Nernst-Planck equations, J. Comput. Electron. 16:431-441(2017).

[27] H. Liu and Z. Wang, A free energy satisfying finite difference method for Poisson-Nernst-Planck equations, J. Comput. Phys. 268:363-376(2014).

[28] M. Metti, J. Xu, and C. Liu, Energetically stable discretizations for charge transport and electrokinetic models, J. Comput. Phys. 306:1–18(2016).

[29] D. He and K. Pan, An energy preserving finite difference scheme for the Poisson-Nernst-Planck system, Appl. Math. Comput. 287:214-223(2015).

[30] M. Metti, J. Xu, and C. Liu, Energetically stable discretizations for charge transport and electrokinetic models, J. Comput. Phys.306:1-18(2016).

[31] M. Mirzadeh and F. Gibou, A conservative discretization of the Poisson-Nernst-Planck equations on adaptive cartesian grids, J. Comput. Phys. 274:633-653(2014).

[32] Y. Qian, C. Wang, and S. Zhou, A positive and energy stable numerical scheme for the Poisson-Nernst-Planck-Cahn-Hilliard equations with steric interactions, J. Comput. Phys. 426:109908(2021).

[33] B. Tu, M. Chen, Y. Xie, L. Zhang, B. Eisenberg, and B. Lu, A parallel finite element simulator for ion transport through three-dimensional ion channel systems, J. Comput. Chem. 287:214-223(2015).

[34] S. Xu, M. Chen, S. Majd, X. Yue, and C. Liu, Modeling and simulating asymmetrical conductance changes in gramicidin pores, Mol. Based Math. Biol. 2:34-55(2014).

[35] D. He, K. Pan, and X. Yue, A positivity preserving and free energy dissipative difference scheme for the Poisson-Nernst-Planck system, J. Sci. Comput. 81:436-458(2019).

[36] H. Liu, H. Yu, Maximum-principle-satisfying third order discontinuous Galerkin schemes for Fokker-Planck equations, SIAM J. Sci. Comput. 36(5):A2296-A2325(2014).

[37] H. Liu, W. Maimaitiyiming, Efficient, Positive, and Energy Stable Schemes for Multi-D Poisson-Nernst-Planck Systems, J. Sci. Comput. 87:92(2021).

[38] H. Liu, Z. Wang, P. Yin, and H. Yu, Positivity-preserving third order DG schemes for Poisson-Nernst-Planck equations, J. Comput. Phys. 452:110777(2022).

[39] H. Liu, Optimal error estimates of the direct discontinuous Galerkin method for convection–diffusion equations, Math. Comput. 84:2263-2295(2015).

[40] C. Chen and S. Hu, The highest order superconvergence for bi-k degree rectangular elements at nodes: A proof of 2k-conjecture, Math. Comput. 82(2013).

[41] Susanne C. Brenner and L. Ridgway Scott, The mathematical theory of finite element methods, third edition, Springer, 2009.

[42] W. Cao, H. Liu and Z. Zhang, Superconvergence of the direct discontinuous Galerkin method for convection-diffusion equations, Numer. Meth. Part. D. E.33(2017).

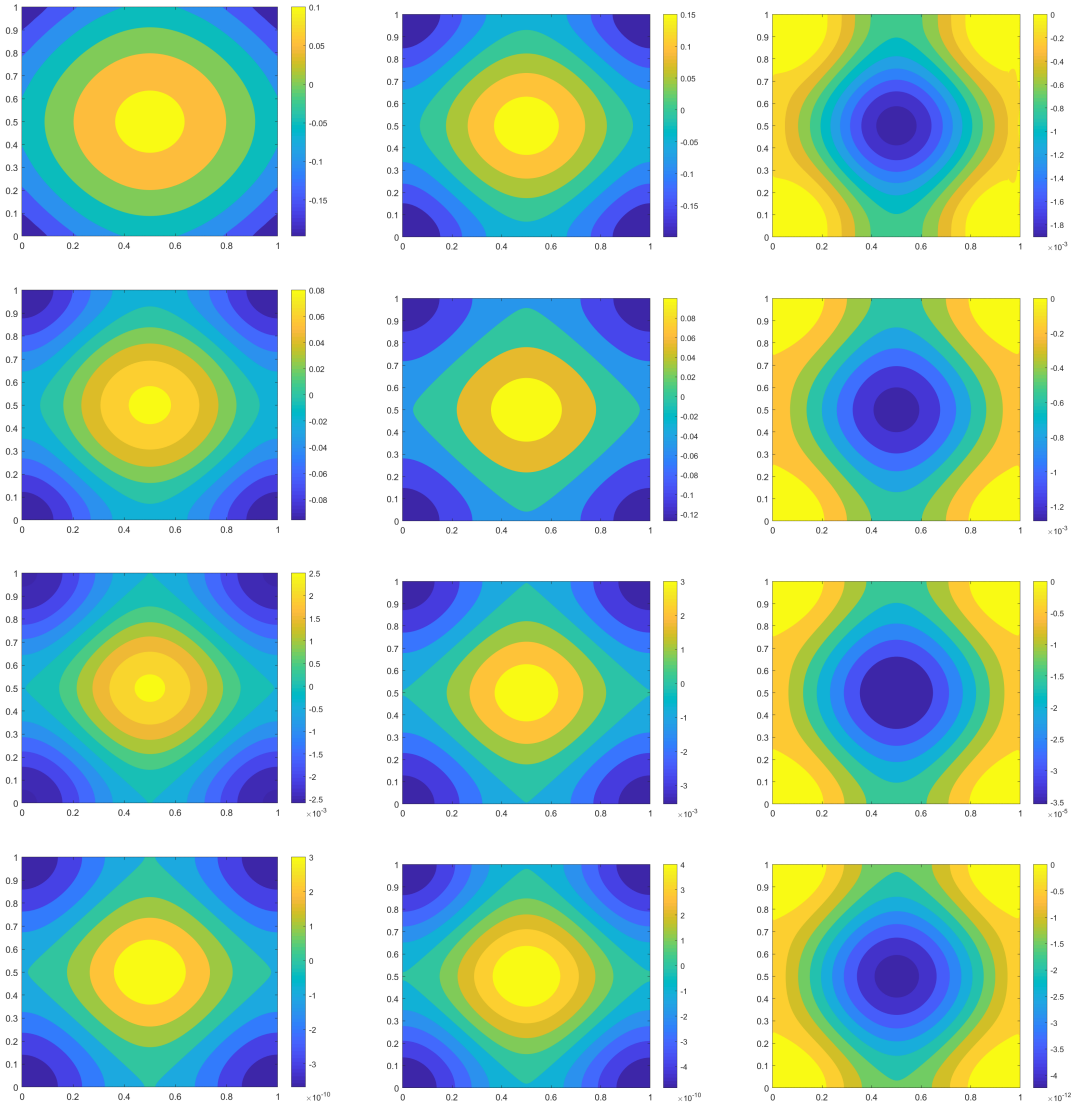

Fig. 6.3. Example 6.3, Numerical solutions of $c_1 - 0.2$(left), $c_2 - 0.2$(middle) and ϕ(right) at $t = 0, 0.01, 0.1$ and $t = 0.5$

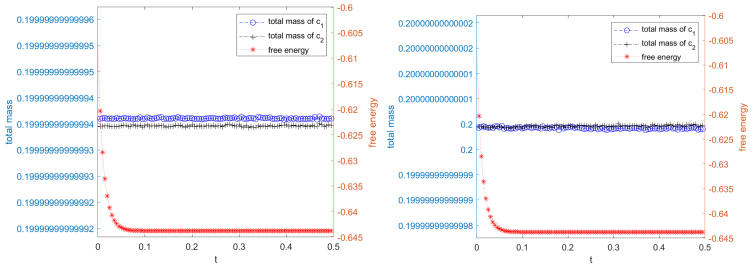

Fig. 6.4. Example 6.3, Temporal evolution of mass and free energy of the numerical solution